



# OPEN Mechanism of reverse deformation increase in the virgin coal rib compared to the pillar rib of the gob-side entry in an extra-thick coal seam

Wenrui He<sup>1,2</sup>, Dongdong Chen<sup>3</sup> & Hengzhong Zhu<sup>4</sup>

The advantage of applying gob-side entries (GSEs) with narrow coal pillars in extra-thick coal seams to improve the recovery rate is particularly significant. However, the ground pressure is intense and overlying strata caving is severe under fully mechanized top-coal caving mining (FMTCM) in extra-thick coal seams. The ground pressure environment of the surrounding rock in GSE with narrow coal pillars is complex, leading to the phenomenon of reverse deformation increase (RDI) where the failure of the virgin coal rib is greater than that of the coal pillar rib. To reveal the mechanism of RDI, this study takes the GSE of the Panel 8211 under typical FMTCM in an extra-thick coal seam as the engineering background. Through on-site measurements of the surface convergence of the GSE ribs, damage of support structures, coal mass damage depth, and abutment stress, as well as numerical analysis of the supporting characteristics of gob gangue on coal pillars, the coal pillar width, and the excavation timing, the following findings are obtained. The support of gangue on the ribs of the coal pillar is the direct cause of RDI. RDI only occurs when the gangue's contact height with the coal pillar exceeds 20 m, while the degree of RDI no longer increases when the contact height exceeds 30 m. On the premise that the gangue's contact height exceeds 20 m, the smaller the coal pillar width or the shorter the lag time between the excavation of the GSE and the completion of mining in the upper panel, the more significant of the RDI. However, coal pillar width and GSE excavation timing only affect the degree of RDI, rather than being preconditions for RDI. To address RDI in GSE with narrow coal pillars under FMTCM in extra-thick coal seams, a support strategy is proposed: reinforcing coal pillars with anchor cables to share the ground pressure on the virgin coal rib, while simultaneously using anchor cables to strengthen the control of deformation in the virgin coal rib. This measure has achieved satisfactory results in practice, and the overall deformation of the GSE meets the requirements of safe production.

**Keywords** Extra-thick coal seam, Coal pillar, Gob-side entry, Reverse deformation increase, Gangue, Excavation timing

China has abundant reserves of extra-thick coal seams with thickness exceeding 8 m, which account for over 45% of total coal output. These seams are concentrated in Shanxi, Shaanxi, Inner Mongolia, and Xinjiang, serving as the primary mining coal seams for coal mines with an annual production capacity exceeding ten million tons<sup>1</sup>. The fully mechanized top-coal caving mining (FMTCM) method for extra-thick coal seams is widely employed in major mining areas across China, leading the coal industry in terms of productivity, efficiency, and comprehensive economic benefits<sup>2</sup>. However, the coal-bearing strata where extra-thick coal seams occur are weak, soft, deeply buried, and subjected to ultra-large mining scale. These factors lead to extremely intense ground pressure behavior, which severely hinders safe and efficient mining operations. This issue has emerged

<sup>1</sup>School of Civil Engineering and Architecture, Jiaying Nanhu University, Jiaying 314001, China. <sup>2</sup>School of Mines, China University of Mining and Technology, Xuzhou 221116, China. <sup>3</sup>School of Energy and Mining Engineering, China University of Mining and Technology (Beijing), Beijing 100083, China. <sup>4</sup>State Key Laboratory of Disaster Prevention and Ecology Protection in Open-pit Coal Mines, Qindao 266590, China. ✉email: 15162178421@163.com; skd996317@sdust.edu.cn

as one of the foremost challenges in mining science and ground control engineering<sup>3</sup>. Particularly the gob-side entries (GSEs) in extra-thick coal seams are adjacent to vast mined-out areas. The overlying strata undergo intense fracturing, causing the peak abutment pressure zone to shift significantly inward. This results in extensive and severe damage of the coal-rock mass on the ribs of the GSE, leading to instability or even closure of the surrounding rock. Consequently, both the difficulty and cost of control measures increase substantially.

GSEs often exhibit asymmetric damage, that is, the deformation and failure of the coal rib, roof and floor on the coal pillar side are greater than those of the virgin coal side. Peng et al.<sup>4</sup> found that the deformation of the coal pillar rib is greater than that of the virgin coal rib under different coal pillar widths, while the rib deformation of the coal pillar and virgin coal can reduce with the coal pillar width. Yang et al.<sup>5</sup> observed that the support structures on the gob-side exhibited prominent splitting failure, accompanied by roof subsidence and floor heave in large-section GSEs. The ground pressure manifestations in coal pillar side were more severe compared to the virgin coal side. For inclined coal seams, the asymmetric deformation of the surrounding rock of GSEs is further amplified. Wang et al.<sup>6</sup> found that the failure of the surrounding rock on the coal pillar rib was significantly greater than that on the virgin coal rib in inclined coal seams, and the peak abutment pressure on the virgin coal rib was 4.2 MPa higher than that on the coal pillar rib. Wu et al.<sup>7</sup> presented that the deflection of the gravity center of the roof toward the gob was identified as the leading cause of asymmetric failure in GSEs in inclined coal seams. Zhu et al.<sup>8</sup> pointed out that the mining-induced pressure in GSEs exhibits an asymmetric distribution, where the pressure on the uncut roof side is significantly higher than that on the roof-cutting side when applying the pressure relief technique by roof cutting.

Research on the mechanism of surrounding rock failure and instability in GSEs still inherits and applies some classic roadway failure theories, such as the arch theory<sup>9–11</sup>, the elastoplastic failure theory<sup>12</sup>, and the surrounding rock loose circle theory<sup>13</sup>. Based on the particularity of the mining environment where GSEs are located, existing studies generally analyze the ground pressure through the rock strata above GSEs to explore the mechanism of surrounding rock failure. Among them, the key block structure on the gob-side<sup>14–17</sup> and the cantilever beam structure<sup>18</sup> are the most widely applied. Meanwhile, numerous studies have confirmed that the position of the fracture line of the overlying main roof relative to the GSE has a significant impact on the stability of their surrounding rock<sup>19–21</sup>. Additionally, based on the main roof fracture line, the stress of the coal mass on the gob-side is divided into two distinct stress environments: internal field and external field<sup>22,23</sup>.

Regarding the mechanism of asymmetric deformation and failure in GSEs, Wang et al.<sup>24</sup> revealed that the main roof above the GSEs forms a hinged structure, attributing the greater deformation of the coal pillar rib compared to the virgin coal rib to the rotation of key blocks. Li et al.<sup>25</sup> concluded that when a GSE is excavated before the movement of the overlying strata stabilizes, the roof experiences rapid subsidence, the stress in the coal pillar increases sharply, and significant asymmetric deformation occurs. The asymmetric failure of GSEs manifests bidirectionally in both vertical and horizontal directions. Xu et al.<sup>26</sup> pointed out that the heterogeneity of surrounding rock stress is the cause of asymmetric failure in GSEs. Meanwhile, the fracture position of the main roof correlates strongly with the asymmetric deformation observed in GSEs<sup>27</sup>. Some scholars have revealed that GSEs exhibit a distinctly asymmetric stress distribution under combined dynamic and static loads<sup>28</sup>. Their studies show a significant negative correlation between the overlying loads on the coal pillar rib and the virgin coal rib, which leads to asymmetric failure of the surrounding rock<sup>29</sup>. Liu et al.<sup>30</sup> presented that the stress concentration and the expansion of the failure zone width in coal pillar are identified as the root causes of the intensified deformation of the surrounding rock on the coal pillar rib.

Among the analysis indicators for the surrounding rock deformation and failure of the GSE, abutment pressure is commonly used to evaluate the surrounding rock stress environment of GSEs due to its ease of monitoring<sup>31–35</sup>. GSEs are subjected to multiple mining dynamic pressure influences. Therefore, dynamic loads and static loads are also widely used to analyze the strata pressure characteristics of GSEs<sup>36,37</sup>. Besides this, some studies explore the mechanism of surrounding rock failure from the perspective of deviatoric stress<sup>38,39</sup> or principal stress<sup>40</sup>.

The above studies focus on the traditional asymmetric deformation, where the deformation of the coal pillar rib is greater than that of the virgin coal rib. Our research team found in the ground pressure observation of GSEs with 8 m narrow coal pillars in extra-thick coal seams of 15 m that after a period of the GSE excavation, the deformation of the virgin coal rib exceeds that of the coal pillar rib. Distinct from the traditional asymmetric deformation characterized by greater deformation of the coal pillar rib, a special ground pressure phenomenon of reverse deformation increase (RDI) has been identified. However, there are currently no relevant studies that reveal the mechanism of RDI. Through on-site monitoring and numerical simulations, this study clarifies the engineering geological conditions for the occurrence of RDI and reveals its generation mechanism from the perspectives of the contact condition between gob gangue and the coal pillar, coal pillar width, and excavation timing.

## Project overview

Panel 8211 is adjacent to the gob of Panel 8210, which has been fully mined and is now stable. To the east lies the protective coal pillar for the village. To the north are the planned but not yet mined Panels N8205 and N8206. Panel 8211 is separated from the gob of Panel 8210 by an 8 m narrow coal pillar, as shown in Fig. 1.

The coal seam mined in Panel 8211 is the #3–5 coal seam, with an average thickness of 15.1 m, classifying it as an extra-thick coal seam. The coal seam is buried at a depth of 415 m, and has an average dip angle of 2.5°. The immediate roof of the coal seam consists of mudstone and fine sandstone, while the main roof consists of medium coarse sandstone with a thickness of 14.7 m, as shown in Fig. 2. Panel 8211 is laid out along the floor of the coal seam and adopts the FMTCM technology to extract the extra-thick coal seam. The mechanized mining height is 3.9 m, with the caving height is approximately 11 m.

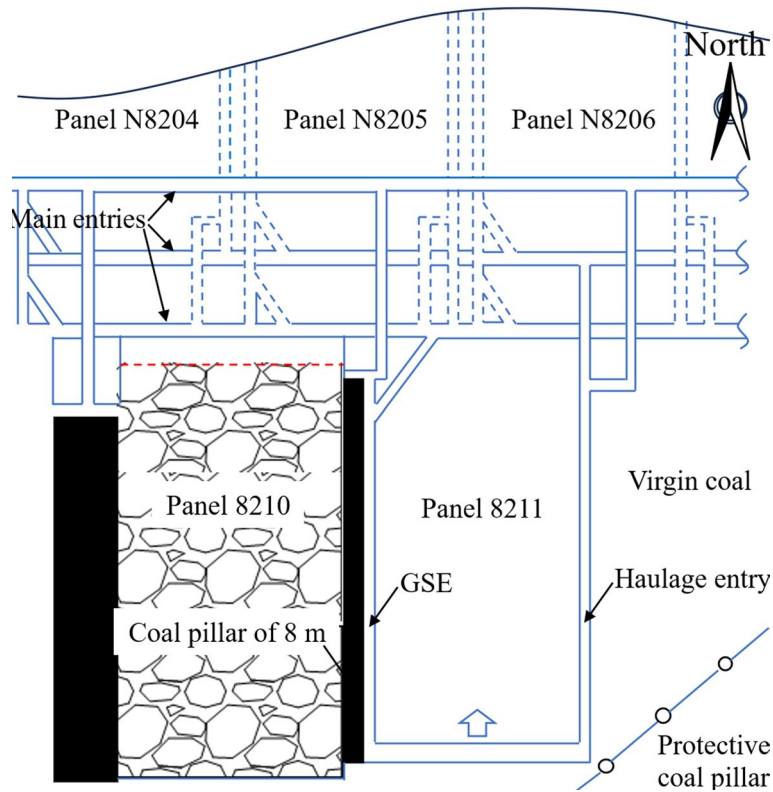


Fig. 1. Location and mining condition of the Panel 8211.

Lithology	Rock core	Thickness/m
Interbedding layer of sandy mudstone and aluminous mudstone		34
Medium coarse sandstone		9.2
Interbedding layer of mudstone and fine sandstone		56.9
Medium coarse sandstone		14.7
Fine sandstone		3.2
Mudstone		2.3
Coal seam		15.1
Mudstone		5.3
Fine sandstone		14.5

Fig. 2. Stratigraphic column of coal-bearing strata.

The GSE of Panel 8211 is driven along the floor of the coal seam, with an 8 m coal pillar between the GSE and the gob. The GSE cross-section measures 6 m × 4 m. In the original support design, the roof is supported with bolts, channel steel beams combined with anchor cables, and cable truss structures. The coal pillar rib is supported with bolts and anchor cables, where the anchor cables are arranged in a staggered pattern with one per row. The virgin coal rib is supported with bolts and ladder beams. The detailed support scheme and parameters are illustrated in Fig. 3.

**Ground pressure behavior of GSE ribs in extra-thick coal seam**  
**Deformation and failure characteristics of the GSE ribs**

During the GSE development in the Panel 8211, intense ground pressure behavior was observed. As soon as the GSE was excavated, the surrounding rock of the coal pillar rib exhibited extensive failure characteristics. Bolt and cable drill holes were damaged and prone to collapse, making it difficult to install resin cartridges,

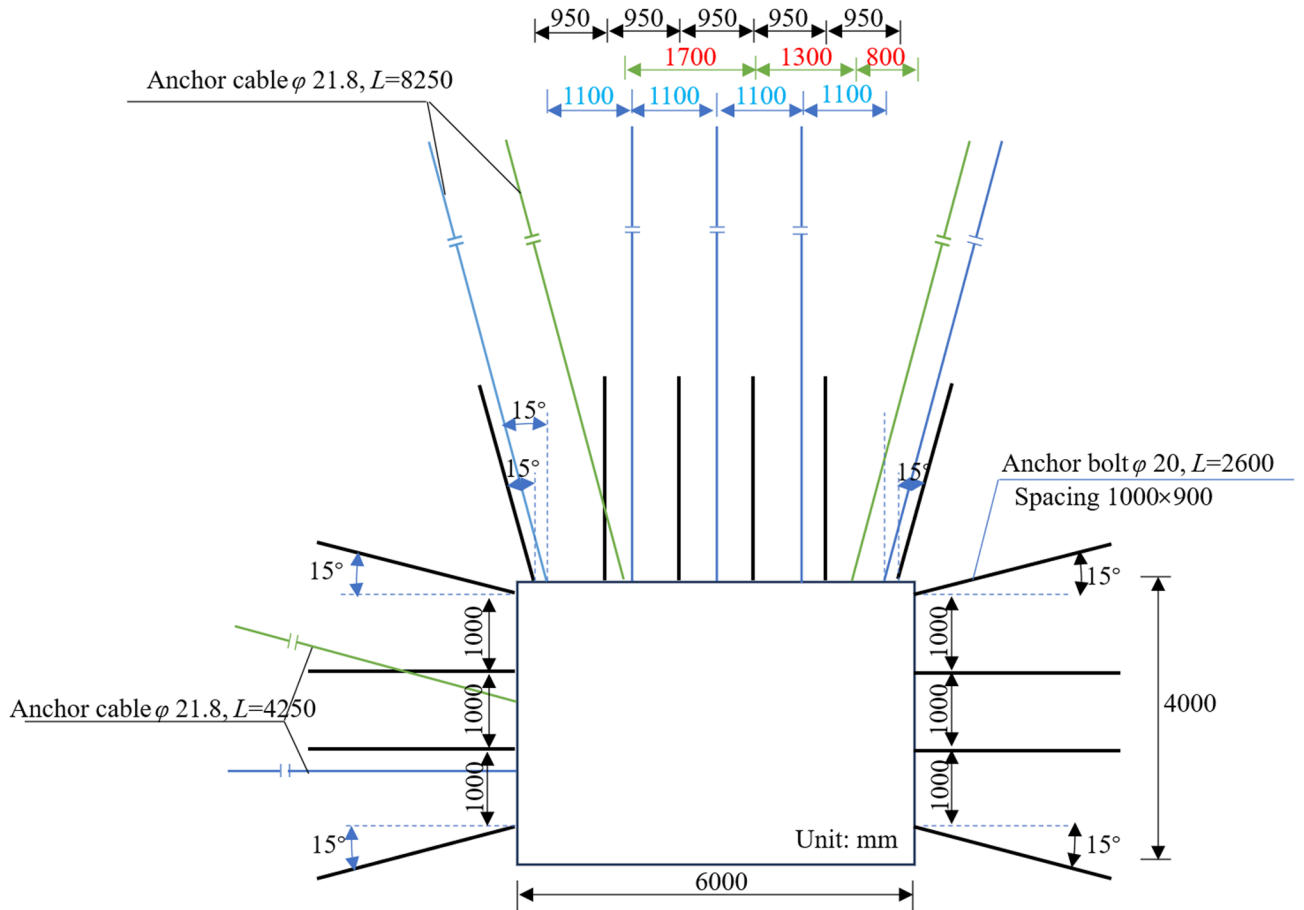


Fig. 3. Original supports of the GSE.

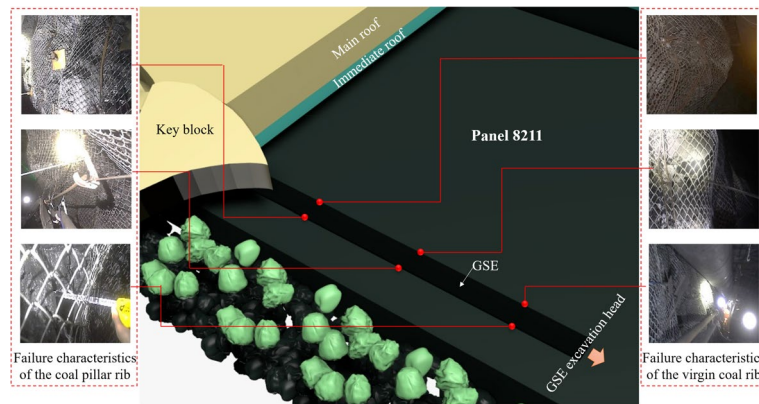


Fig. 4. Deformation and failure characteristics of the surrounding rock at the GSE ribs.

bolts, and cables. A period after GSE excavation, fractures in the coal ribs developed intensely and continued to propagate and extend. The coal pillar rib was significantly displaced inward the GSE, and the virgin coal rib also experienced severe convergence. The deformation and failure of the surrounding rock seriously compromised the functionality of the GSE for ventilation, personnel passage, and transport, as well as the safe and efficient production during the mining, as shown in Fig. 4.

Two monitoring stations were established in the trial excavation section of the GSE to monitor the deformation of the surrounding rock. The distances from Monitoring Station #1 and #2 to the excavation portal are 15 m and 30 m, respectively. The monitoring results, shown in Fig. 5, indicate that in the early excavation stage, the deformation of the coal pillar rib was greater than that of the virgin coal rib. However, after 30 days, the deformation rate of the virgin coal rib increased significantly, and by approximately 50 days, its cumulative

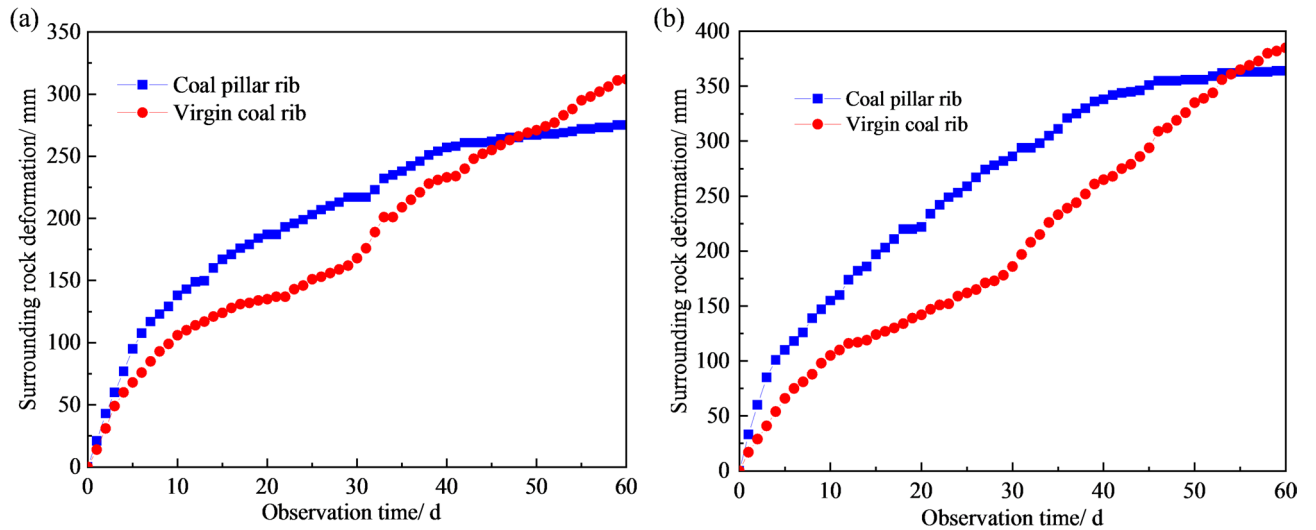


Fig. 5. Surrounding rock deformation of ribs in the GSE: (1) Station #1; (2) Station #2.

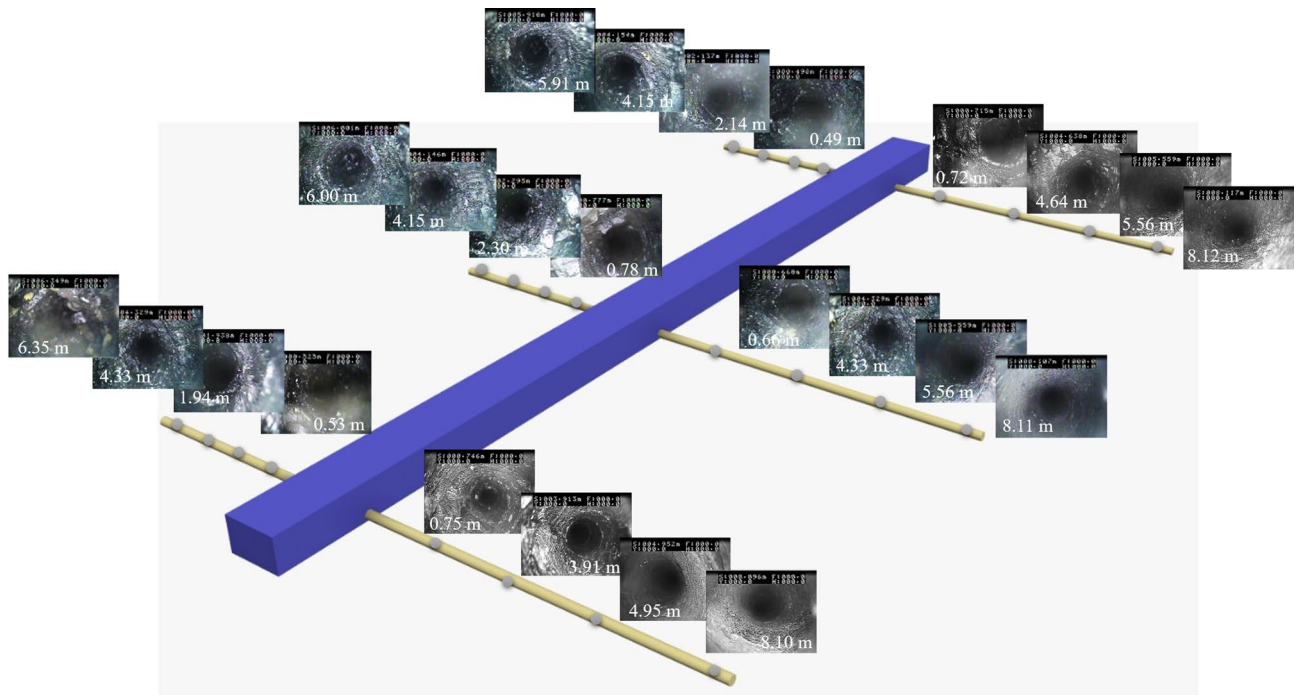


Fig. 6. Depth and degree of the rib failure by borehole television.

deformation exceeded that of the coal pillar rib. Contrary to the traditional asymmetric deformation in GSEs where the coal pillar rib deforms more than the virgin coal rib, the GSE of Panel 8211 exhibited the RDI. Furthermore, under the original support conditions, the GSE continued to deform for two months without showing signs of stabilization.

**Failure degree of the GSE ribs**

The Failure degree of the GSE ribs by borehole television results is shown in Fig. 6; Table 1. The results indicate that the coal mass around the 6.5 m borehole in the coal pillar rib has suffered different degrees of damage. As the coal pillar undergoes bidirectional deformation and damage on both the gob-side and the GSE side, this indicates that the entire 8 m coal pillar is damaged. Meanwhile, the damage degree of the coal mass in the coal pillar on the gob-side and the GSE side is more severe than that in the middle. The average range of the failure zone in the virgin coal side is 4.29 m, and the failure degree of the shallow coal mass is greater than that of the deep coal mass. The above results show that under the original support conditions, the surrounding rock of the

Surrounding rock	Fracture intensity	Failure degree	Average failure degree
Coal pillar rib	Strong	Overall failure	8.00 m
Virgin coal rib	Strong	3.91–4.64 m	4.29 m

**Table 1.** Failure extent of surrounding rock in the ribs.

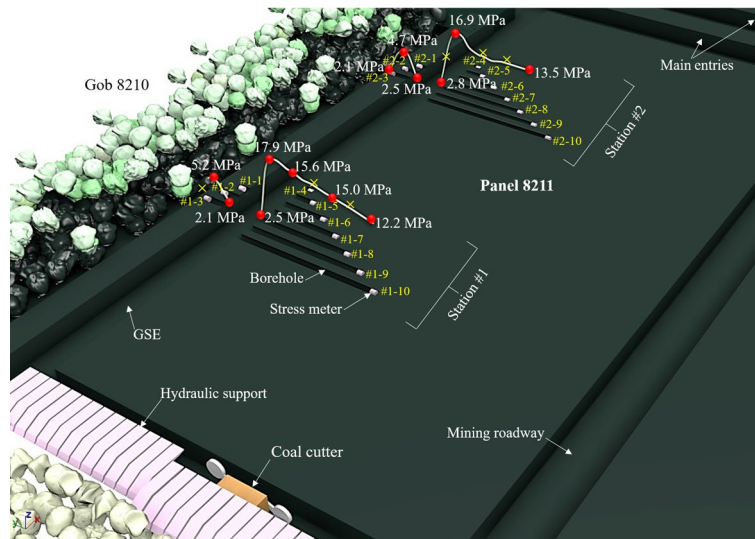


**Fig. 7.** Abutment stress characteristics in the rib.

	Abutment stress in pillar/ MPa			Abutment stress in virgin coal rib/ MPa						
	#1-1	#1-2	#1-3	#1-4	#1-5	#1-6	#1-7	#1-8	#1-9	1-10#
Station #1	2.1	5.2	/	2.5	17.9	15.6	/	15.0	/	12.2
Station #2	#2-1	#2-2	#2-3	#2-4	#2-5	#2-6	#2-7	#2-8	#2-9	2-10#
	2.5	4.7	2.1	2.8	/	16.9	/	/	13.5	/

**Table 2.** Abutment stresses of borehole meters.

GSE ribs with narrow coal pillars in the extra-thick coal seam under FMTCM has a large loose zone, a wide damage range and a high damage degree.

### Abutment stress in the coal rib

Due to missing abutment stress data from individual damaged stress meters at monitoring stations, the analysis was performed by combining results from Station #1 and #2, as shown in Fig. 7; Table 2. The abutment stress distribution exhibits a significantly asymmetric characteristic between the coal pillar and the virgin coal rib. The abutment stress in the center of the 8 m coal pillar is greater than that on its two sides, with an average peak value of 4.95 MPa. The peak abutment stress in the virgin coal rib is located in boreholes #1–5, at a distance of 6 m from the virgin coal rib surface. The stress gradually decreases with increasing distance from the virgin coal rib. The abutment stress recorded in boreholes #1–10 is 12.2 MPa, a value close to the initial in-situ stress of the coal seam. These findings indicate that in GSEs with narrow coal pillars under the condition of FMTCM in extra-thick coal seams, both the coal pillars and the shallow virgin coal ribs have suffered severe damage, while the deep zone of the virgin coal ribs bears higher stress.

### RDI mechanism Numerical models

A global numerical model was established using FLAC<sup>3D</sup>. The model dimensions are 900 m × 600 m × 154 m. The dip length of the mined-out Panel 8210 is 220 m, and the strike length is 800 m. Displacements were fixed at the bottom. Four lateral boundaries of the model are roller supports, while an overburden load of 7.4 MPa was applied to the top. Based on the engineering and geological condition of the Panel 8210 and 8211, a physical model was built to determine the fracture parameters of the overlying strata. It can be observed from the results in Fig. 8 that the overburden fracture height and angle are 77 m and 80°, respectively. The bulking factor of the

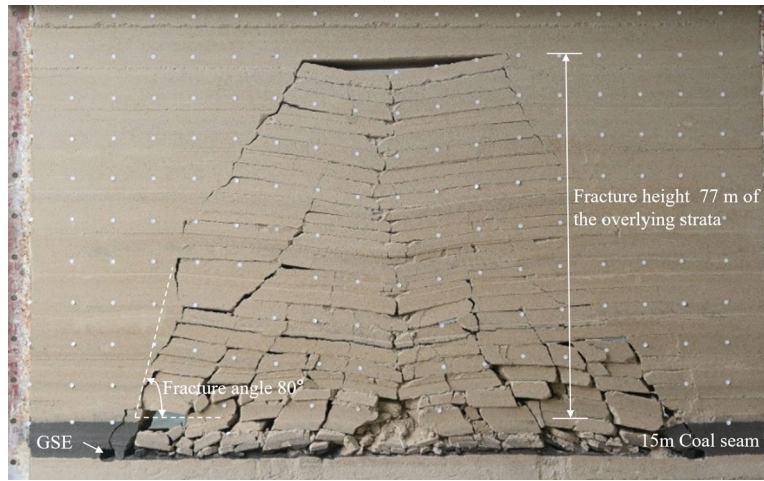


**Fig. 8.** Physical model of the overlying strata fracture characteristics and parameters.

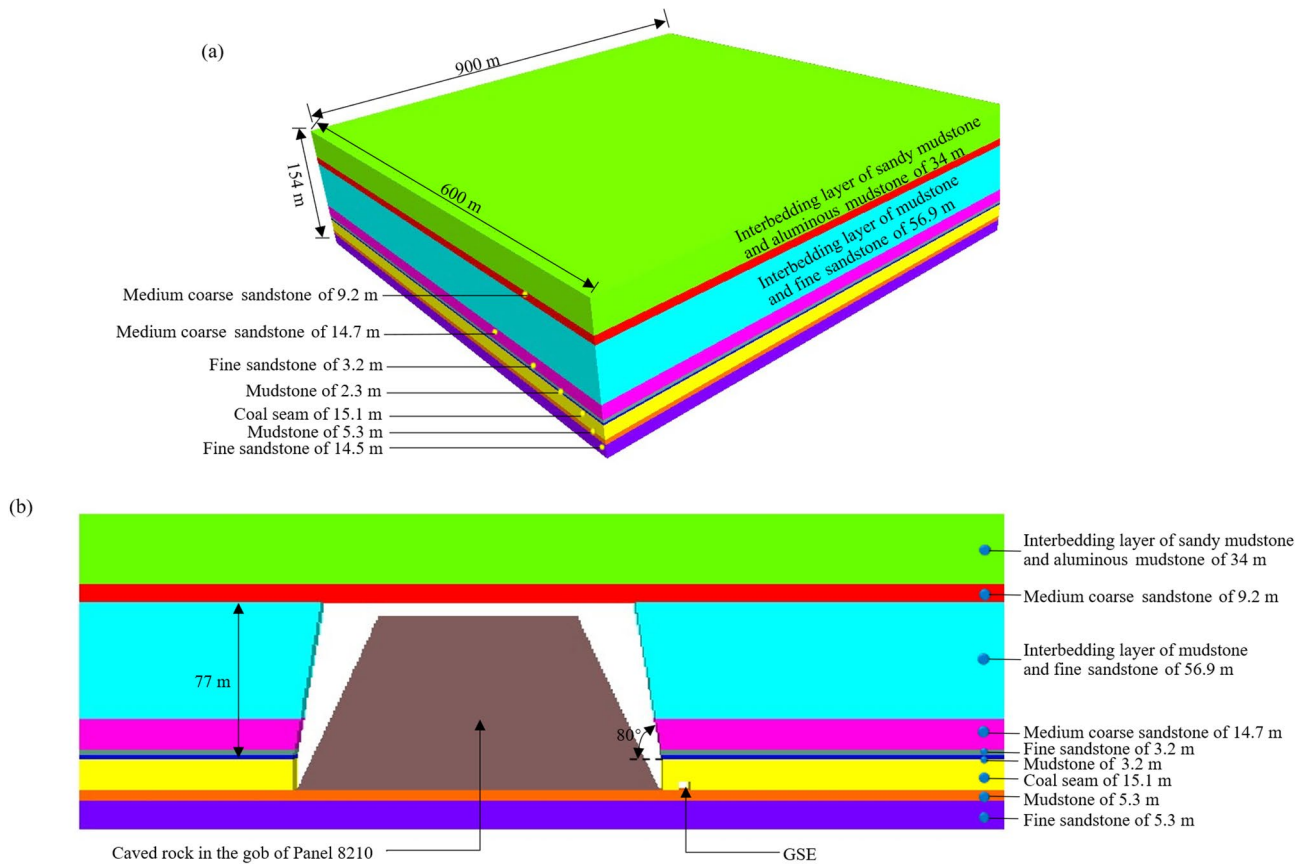


**Fig. 9.** Simulation model: (a) Global model; (b) Model after upper panel and GSE excavation.

gangué is 1.1. In the numerical model, the GSE is supported by bolt-cables, with the support parameters identical to those provided in Fig. 3. The numerical model is illustrated in Fig. 9.

The Mohr-Coulomb constitutive model was employed for the coal and rock masses in the numerical model. The mechanical parameters listed in Table 3 were determined by calibrating the results from laboratory mechanical tests on coal-rock samples. The modified method employs the Hoek-Brown (H-B) criterion, which is expressed as follows<sup>41</sup>:

$$\sigma_1 = \sigma_3 + \sigma_{ci} \left( m_b \frac{\sigma_3}{\sigma_{ci}} + s \right)^a \tag{1}$$

Lithology	Density (Kg/m <sup>3</sup> )	Bulk modulus (GPa)	Shear modulus (GPa)	Cohesive (MPa)	Friction angle (°)
Interbedding layer of sandy and aluminous mudstone	2310	2.26	1.04	0.16	23
Medium coarse sandstone	2540	12.22	8.05	2.60	48
Interbedding layer of mudstone and fine sandstone	2450	7.23	3.20	1.55	31
Medium coarse sandstone	2540	12.22	8.05	2.60	48
Fine sandstone	2180	9.53	5.72	1.87	42
Mudstone	2310	6.26	1.04	1.30	23
Coal seam	1450	2.13	6.46	1.01	19
Mudstone	2310	6.26	1.04	1.30	23
Fine sandstone	2180	9.53	5.72	1.87	42

**Table 3.** Mechanical parameters in the simulation model.

where  $\sigma_{ci}$  is the uniaxial compressive strength of the intact rock;  $\sigma_1$  and  $\sigma_3$  are the maximum and minimum principal stresses, respectively; and  $m_b$ ,  $s$ , and  $a$  are rock mass constants, which are obtained from the following equations:

$$m_b = m_i e^{\frac{GSI-100}{28-14D}} \tag{2}$$

$$s = e^{\frac{GSI-100}{9-3D}} \tag{3}$$

$$a = \frac{1}{2} + \frac{1}{6} \left( \exp\left(-\frac{GSI}{15}\right) - \exp\left(-\frac{20}{3}\right) \right) \tag{4}$$

where  $m_i$  is the intact rock parameter,  $D$  is the disturbance factor, and  $GSI$  denotes the geological strength index. The strength parameters of the cohesion and internal friction angle of coal and rock mass are as follows:

$$\varphi = \sin^{-1} \left[ \frac{3am_i(s + m_i\sigma_{3n})^{a-1}}{(1+a)(2+a) + 3am_i(s + m_i\sigma_{3n})^{a-1}} \right] \tag{5}$$

$$c = \frac{\sigma_{ci}[(1+2a)s + (1-a)m_i\sigma_{3n}](s + m_i\sigma_{3n})^{a-1}}{(1+a)(2+a)\sqrt{\frac{1+(6am_i(s+m_i\sigma_{3n})^{a-1})}{(1+a)(2+a)}}} \tag{6}$$

Herein,  $\sigma_{3n}$  is given by the ratio  $\sigma_{3max}/\sigma_{ci}$ , whereby  $\sigma_{3max}$  corresponds to the upper limit of the minimum principal stress.

The elastic modulus, a key parameter characterizing rock mass deformation, is modified by the disturbance coefficient  $D$  as follows:

$$\begin{cases} E_m = \left(1 - \frac{D}{2}\right) \sqrt{\frac{\sigma_{ci}}{100}} 10^{\frac{GSI-10}{40}} \\ E_m = \left(1 - \frac{D}{2}\right) 10^{\frac{GSI-10}{40}} \end{cases} \tag{7}$$

Given the considerable influence of mining-induced stress on the coal-rock mass,  $D$  is assigned a value of 0.7. The values for  $GSI$  and  $m_i$  are adopted from the tables published by Hoek and Brown<sup>42</sup>.

In the numerical model, the gangue was simulated using the Double-Yield model available in FLAC3D. Based on the on-site measured abutment stress values in the virgin coal rib presented in Table 2 (Sect. 3.3), the goaf gangue parameters were iteratively adjusted using the trial and error method until the abutment stress of the coal seam matched the field-measured data (as shown in Fig. 10), yielding the goaf gangue simulation parameters listed in Tables 4 and 5.

Meanwhile, it can be seen from Fig. 10 that the distribution characteristics of the abutment stress in the virgin coal rib obtained from the numerical simulation agree well with the field measurements. Specifically, the simulated and measured peak abutment stress values are 18.11 MPa and 17.90 MPa, respectively, with an error of only 1.17%. The corresponding positions of the peak stress are 6.49 m and 6.00 m, yielding an error of 8.16%. Additionally, at a distance of 11 m from the coal rib, the field-measured abutment stress is 15.60 MPa, while the numerical simulation result is 16.11 MPa, corresponding to an error of 3.7%. These results demonstrate that the parameters, constitution relations, and boundary conditions adopted in the numerical model are reasonable and reliable.

Numerical simulation procedure is as follows:

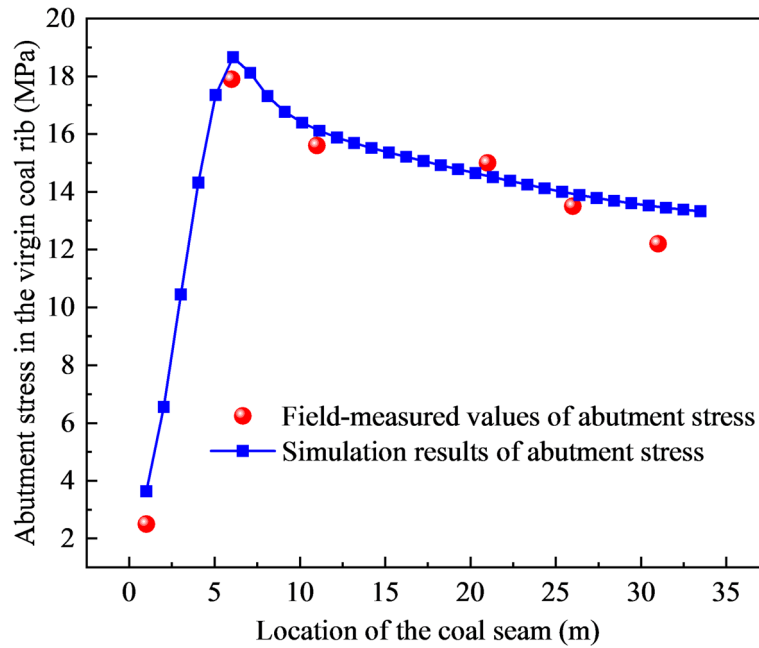


**Fig. 10.** Numerical model parameters determination and verification.

Mechanical parameters	Bulk modulus (GPa)	Shear modulus (GPa)	Tensile strength (MPa)	Cohesion (MPa)	Friction angle (°)	Dilation angle (°)
Value	5.0	2.08	0.1	9.76	28	7

**Table 4.** Mechanical parameters of the gangue.

Strain	0.01	0.02	0.05	0.1	0.15	0.18
Cap pressure (MPa)	0.17	0.37	1.13	3.52	11.9	57.0

**Table 5.** Cap pressure in the gangue.

- Construct the model, divide the mesh, specify the constitutive relations, and assign material parameters.
- Run the global model until the rock strata subsidence stabilizes.
- Excavate the tailgate and headgate of Panel 8210, and achieve stress equilibrium.
- Mine the Panel 8210 until the specified calculation steps are completed.
- Develop the GSE of Panel 8211.
- Analyze the stress and deformation characteristics of the surrounding rock.

To investigate the influencing factors and mechanisms of the RDI observed at the coal ribs of the GSE in an extra-thick coal seam with FMTCM, three distinct simulation schemes were established, as detailed in Table 6.

Scheme 1 focuses on the contact height of caved gangue with the gob-adjacent coal pillar rib. The coal pillar width is 8 m, and the time interval between GSE excavation and the completion of mining in the upper panel is  $2.0 \times 10^4$  calculation steps, i.e., the overlying strata of the upper panel have been stable. Five different contact heights were simulated: 0 m (Group A-1), 10 m (Group A-2), 20 m (Group A-3), 30 m (Group A-4), and 40 m (Group A-5).

Scheme 2 investigates the effect of coal pillar width. The contact height of the gangue is fixed at 30 m, and the GSE is driven at  $2.0 \times 10^4$  steps after mining the upper panel. Five different coal pillar widths were analyzed: 5 m (Group B-1), 10 m (Group B-2), 20 m (Group B-3), 30 m (Group B-4), and 40 m (Group B-5).

Scheme 3 examines the timing of GSE development. The coal pillar width is fixed at 8 m and the gangue contact height is fixed at 30 m. Five different excavation timing scenarios were studied, corresponding to different calculation steps after the upper panel was mined:  $5 \times 10^3$  steps (Group C-1),  $1 \times 10^4$  steps (Group C-2),  $1.5 \times 10^4$  steps (Group C-3),  $2 \times 10^4$  steps (Group C-4), and  $2.0 \times 10^4$  steps (Group C-5).

	Group A-1	Group A-2	Group A-3	Group A-4	Group A-5
Plan 1	Contact height 0 m of Gangue with coal rib	Contact height 10 m of Gangue with coal rib	Contact height 20 m of Gangue with coal rib	Contact height 30 m of Gangue with coal rib	Contact height 40 m of Gangue with coal rib
	Group B-1	Group B-2	Group B-3	Group B-4	Group B-5
Plan 2	Coal pillar width of 5 m	Coal pillar width of 10 m	Coal pillar width of 20 m	Coal pillar width of 30 m	Coal pillar width of 40 m
Plan 3	The GSE is excavated at 1000 step after the upper panel is completed	The GSE is excavated at 5000 step after the upper panel is completed	The GSE is excavated at 10000 step after the upper panel is completed	The GSE is excavated at 15000 step after the upper panel is completed	The GSE is excavated at 20000 step after the upper panel is completed

**Table 6.** Numerical study schemes.

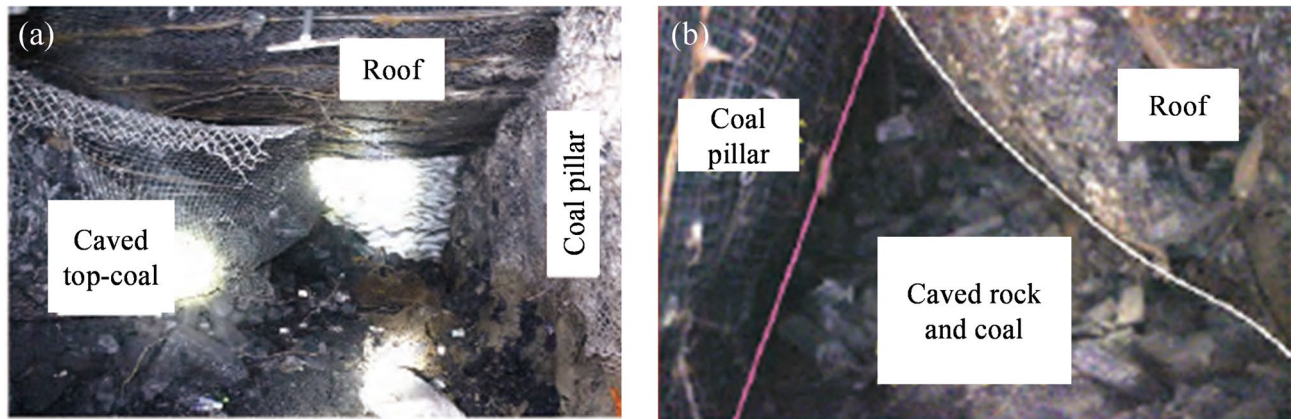


**Fig. 11.** Contact characteristics between the gangue and the gob-side rib of the coal pillar: (a) No contact; (b) In contact<sup>44</sup>.

### Results analysis

#### *Influence of gob gangue on RDI*

Studies has revealed that under the conditions of FMTCM in extra-thick coal seams, the gangue significantly influences the deformation of the coal ribs in GSEs<sup>43</sup>. Based on the actual contact characteristics observed in practical engineering, the conditions are categorized into two types depending on whether the caved gangue is in contact with the gob-side rib of the coal pillar or not, as illustrated in Figs. 11(a) and 11(b), respectively.

Based on the simulation results of different gangue-to-rib contact heights as presented in Fig. 12, it is observed that when the gangue is not in contact with the coal rib (Group A-1) or the contact height is low (Group A-2), the deformation of the pillar rib in the GSE exceeds that of the virgin coal rib, exhibiting the traditional asymmetric failure characteristics. However, when the contact height reaches 20 m or more (Group A-3, A-4, and A-5), the deformation of the virgin coal rib becomes greater than that of the pillar rib, demonstrating the RDI characteristic.

To quantitatively describe the degree of the RDI in the GSE, the RDI rate  $r$  is proposed, which is defined by Eq. (8). When the gangue contact height is 20 m, the RDI value at the central axis position of ribs is 43 mm, resulting in a RDI rate of 66.5%. When the contact height increases to 30 m, the RDI value at the central axis of ribs reaches 49 mm, with a corresponding RDI rate of 84.1%. Furthermore, at a contact height of 40 m, the RDI value is 53 mm, yielding an RDI rate of 83.0%.

$$r = \frac{d_v - d_c}{d_c} \times 100\% \tag{8}$$

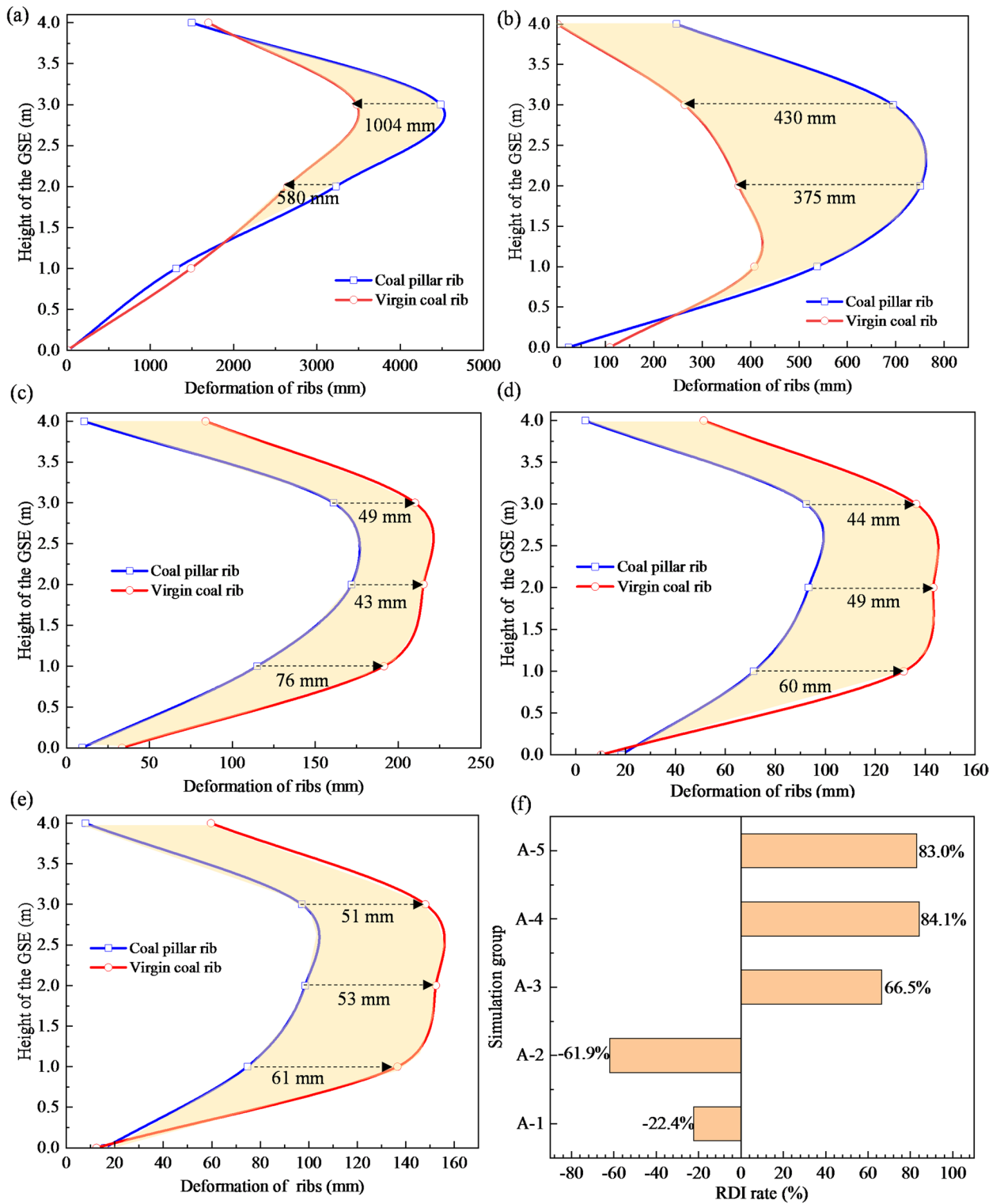


**Fig. 12.** Deformation characteristics of ribs under different gangue support conditions: (a) Group A-1; (b) Group A-2; (c) Group A-3; (d) Group A-4; (e) Group A-5; (f) RDI rate at the central axis position of the rib.

where  $d_v$  is the deformation of the virgin coal rib, and  $d_c$  is the deformation of the coal pillar rib.

The above data indicate that the contact height of caved gangue with the coal rib is a key factor leading to the RDI. A greater contact height results in a higher degree of RDI. However, the degree of RDI does not increase indefinitely with the contact height; once the contact height reaches a certain value, the RDI degree remains essentially constant.

To investigate the mechanism of how gangue influences the deformation of the GSE, the abutment stress and the lateral support force exerted by the gangue on the coal ribs were monitored at the model cross-section of 450 m along GSE strike direction, as shown in Fig. 13. When the contact height between the gangue and the rib is low (10 m and 20 m), the lateral support force is high at the bottom of the rib but low at the top. In contrast, when the contact height is high, the lateral support force is relatively high at both the top and bottom of the rib but lower in the middle. The peak abutment stress values for the coal pillar rib in Groups A-1 to A-5 are 4.59 MPa, 7.46 MPa, 9.21 MPa, 8.85 MPa, and 9.01 MPa, respectively. The corresponding peak values for the virgin coal rib are 10.7 MPa, 14.5 MPa, 17.75 MPa, 18.66 MPa, and 18.61 MPa.

Based on the data presented above, it can be concluded that when the gangue contact height is relatively low, the abutment stress on both the coal pillar rib and the virgin coal rib increases with the gangue contact height. However, when the gangue contact height exceeds 20 m, the abutment stress on the ribs shows little further variation. This indicates that the load-bearing capacity of the coal ribs improves as the gangue contact height increases, but ceases to grow further once the gangue contact height reaches a certain level.

Further investigation into the horizontal stress of the coal ribs in the GSE under different gangue contact heights yielded the results shown in Fig. 14. Except for the low horizontal stress in the coal pillar rib observed in Group A-1, the horizontal stress in the coal pillar rib is similar across the other study groups. However, the horizontal stress in the virgin coal rib increases consistently with the contact height of the gangue.

To explore the relationship between the lateral support force of gangue and the abutment stress of the coal seam as well as the horizontal stress, the lateral support force of the GSE is obtained by integrating Eq. (9). Based on the results presented in Fig. 15, the lateral support force provided by the gangue to the gob-side rib of the GSE increases with the height. Specifically, for each additional meter of gangue contact height, the average lateral support force rises by 2.15 MN. Further investigation reveals that when the gangue contact height is less than 20 m, the peak abutment stress in both the coal pillar and the virgin coal rib increases in response to higher lateral support force from the gangue. Nevertheless, when the gangue contact height surpasses 20 m, any additional increase in its lateral support force exerts minimal influence on the peak abutment stress in the coal pillar rib and virgin coal rib. The above findings indicate that the lateral support force of gangue effectively increases the bearing capacity of the GSE ribs, but this improvement plateaus beyond a certain threshold.

Regarding the relationship between the lateral support force of the gangue and the horizontal stress, except for the case where the gangue is in contact with the coal pillar at a height of 0 m (Group 1), the horizontal stress

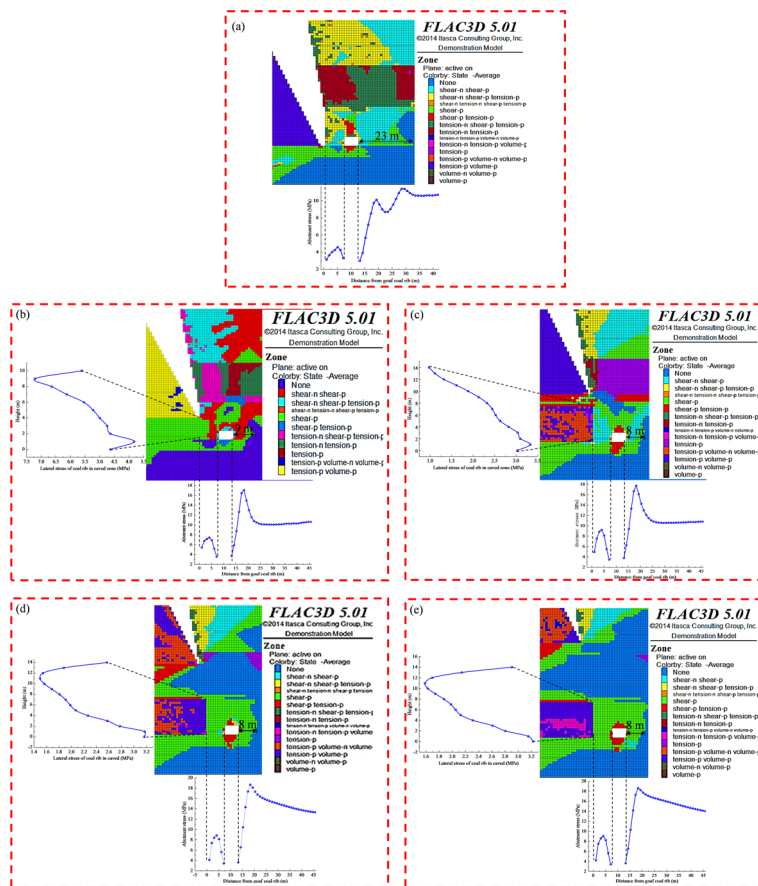


**Fig. 13.** Abutment stress and lateral resistance of the coal pillar under different gangue contact height at location of 450 m along strike direction: (a) Group A-1; (b) Group A-2; (c) Group A-3; (d) Group A-4; (e) Group A-5.

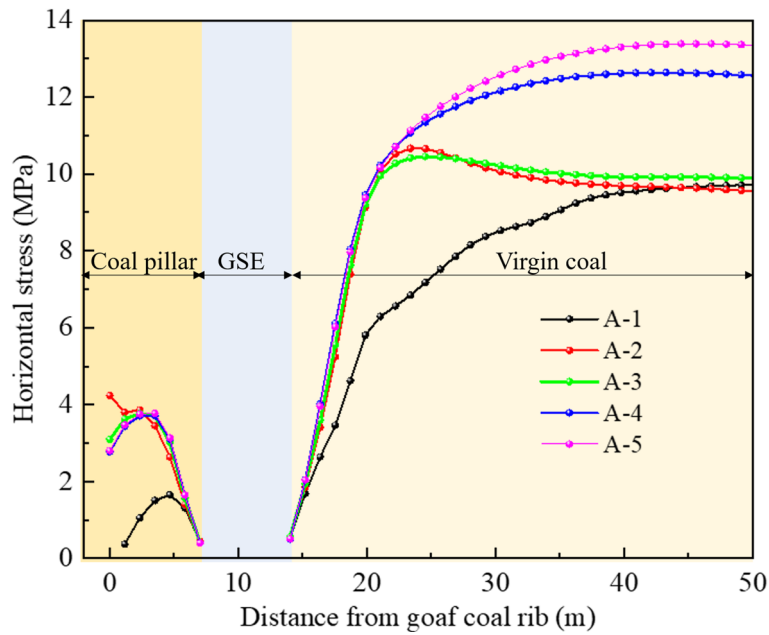


Fig. 14. Horizontal stress of coal ribs in GSE.

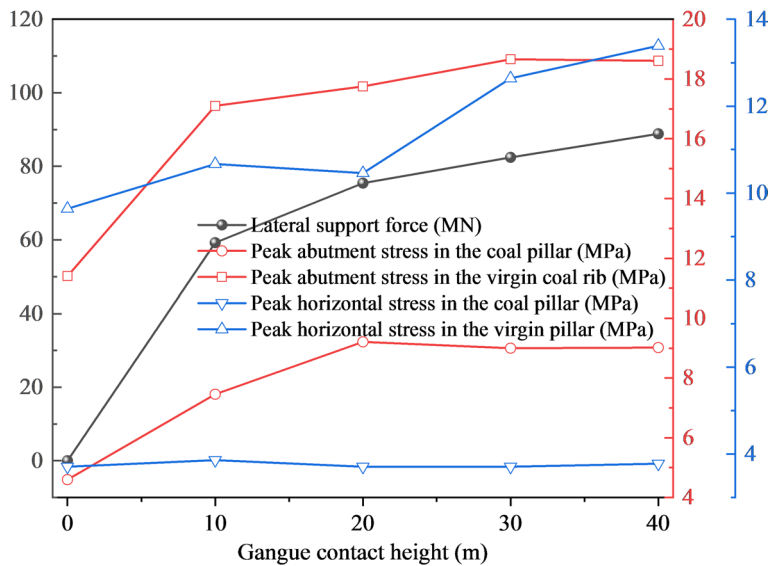


Fig. 15. Relationship between the lateral support force and the abutment stress and horizontal stress.

in the narrow coal pillar exhibits very low sensitivity to changes in the lateral support force from the gangue. In contrast, the horizontal stress in the virgin coal rib increases significantly with higher gangue support force. Specifically, when the lateral support force of the gangue increases from 59.22 MN to 88.82 MN, the horizontal stress in the virgin coal rib rose by 2.72 MPa.

$$F_l = \int_0^{h_1} \sigma_l dh \tag{9}$$

where  $F_l$  denotes the lateral supporting force of gangue on the coal ribs;  $\sigma_l$  represents the lateral supporting stress of gangue;  $h$  and  $h_1$  are the gangue contact heights of the coal rib.

Based on the comprehensive analysis presented above, the influence mechanism of gangue on the RDI can be summarized as follows (Fig. 16): The overlying strata of the GSE can be divided into a damaged zone and an undamaged zone based on their damage degree. The gravity of the rock mass in the damaged zone, along with the overburden load, is transmitted to the coal pillar side. In contrast, the intact rock plate in the undamaged

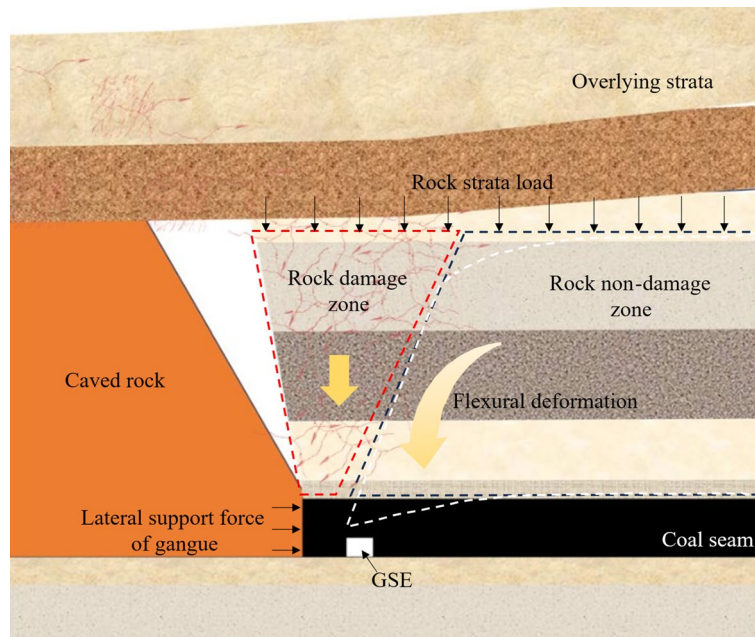


**Fig. 16.** Effect of gangue-to-rib contact height on rib deformation.

zone bends under its own weight and the overburden load, compressing the underlying coal mass and inducing deformation. The gangue provides effective lateral support force to the coal pillar, thereby significantly reducing the damage of the coal pillar. This enhanced support enables the coal pillar to resist the ground pressure from the overlying strata of the damaged zone. The virgin coal rib is situated at the position of maximum deflection of the overlying rock plate, rendering it susceptible to significant deformation. Therefore, for GSEs with narrow coal pillars under FMTCM in extra-thick coal seams, the overlying rock mass sustains extensive and severe damage. The undamaged rock plate migrates toward the virgin coal rib, resulting in increased horizontal stress and abutment stress in the virgin coal rib, subsequently leading to greater deformation of the virgin coal rib. However, the convergence of the coal pillar towards the GSE decreases under the high lateral support force from gangue. Thus, the RDI phenomenon is generated.

#### *Influence of coal pillar width on RDI*

Not only the lateral support force of the gangue but also the coal pillar width determines whether RDI occurs in the GSE. As shown in Fig. 17, when the supporting height of the gangue against the rib is 30 m, GSEs with 5 m and 10 m coal pillars exhibit RDI. The narrower the coal pillar, the greater the RDI magnitude. For a 20 m coal pillar, the deformation of the pillar rib is 16.3 mm greater than that of the virgin coal rib, indicating that RDI does not occur. However, when the pillar width increases to 30 m and 40 m, the deformations of the coal pillar rib and the virgin coal rib tend to be similar.

The abutment stress on the ribs of a GSE comprehensively reflects the damage degree of the rib and the ground pressure transfer characteristics of overlying strata, and directly influences rib deformation. Figure 18 shows the characteristics of the abutment stress in the ribs with different pillar widths at the model cross-section of 450 m along GSE strike direction. The surrounding rock of the ribs in the GSE with the narrow coal pillar suffers a severe damage, and the abutment stresses are primarily determined by the bearing capacity of the damaged coal mass. Consequently, under the condition of a 5 m coal pillar, the peak abutment stress on the coal pillar is only 7.2 MPa, indicating severe failure and large deformation of the coal pillar. As the pillar width increases, the degree of damage to the pillar gradually decreases, and the abutment stress on the coal pillar rises. The wider pillar shares part of the ground pressure originally borne by the virgin coal rib, leading to a reduction in the abutment stress on the virgin coal rib. When the coal pillar width is relatively large (e.g., 30 m and 40 m), the abutment stress and damage degree of the coal pillar rib and the virgin coal rib are close, so the deformation of both ribs is similar (as shown in Fig. 17(c)).

Based on the influence mechanism analysis of the gangue on the deformation and failure of ribs, it is understood that the coal pillars of the GSE with narrow coal pillars are mainly affected by the self-weight of the overlying strata in the damaged zone and the overburden load on it, while the virgin coal rib is squeezed by the flexural deformation of the undamaged overlying rock plate. Under the condition of the gangue height in contact with the pillar rib is large while the width of the coal pillar is small, the RDI phenomenon of the GSEs is likely to occur. In contrast, in a GSE with a wide coal pillar, both the coal pillar rib and the virgin coal rib are located farther away from the influence zones associated with the overlying strata in the damaged zone and the undamaged rock plane. Consequently, the abutment stress on the coal pillars and virgin coal ribs, as well as their damage degrees, are similar, resulting in comparable deformation magnitudes for both ribs, as shown in Fig. 19.

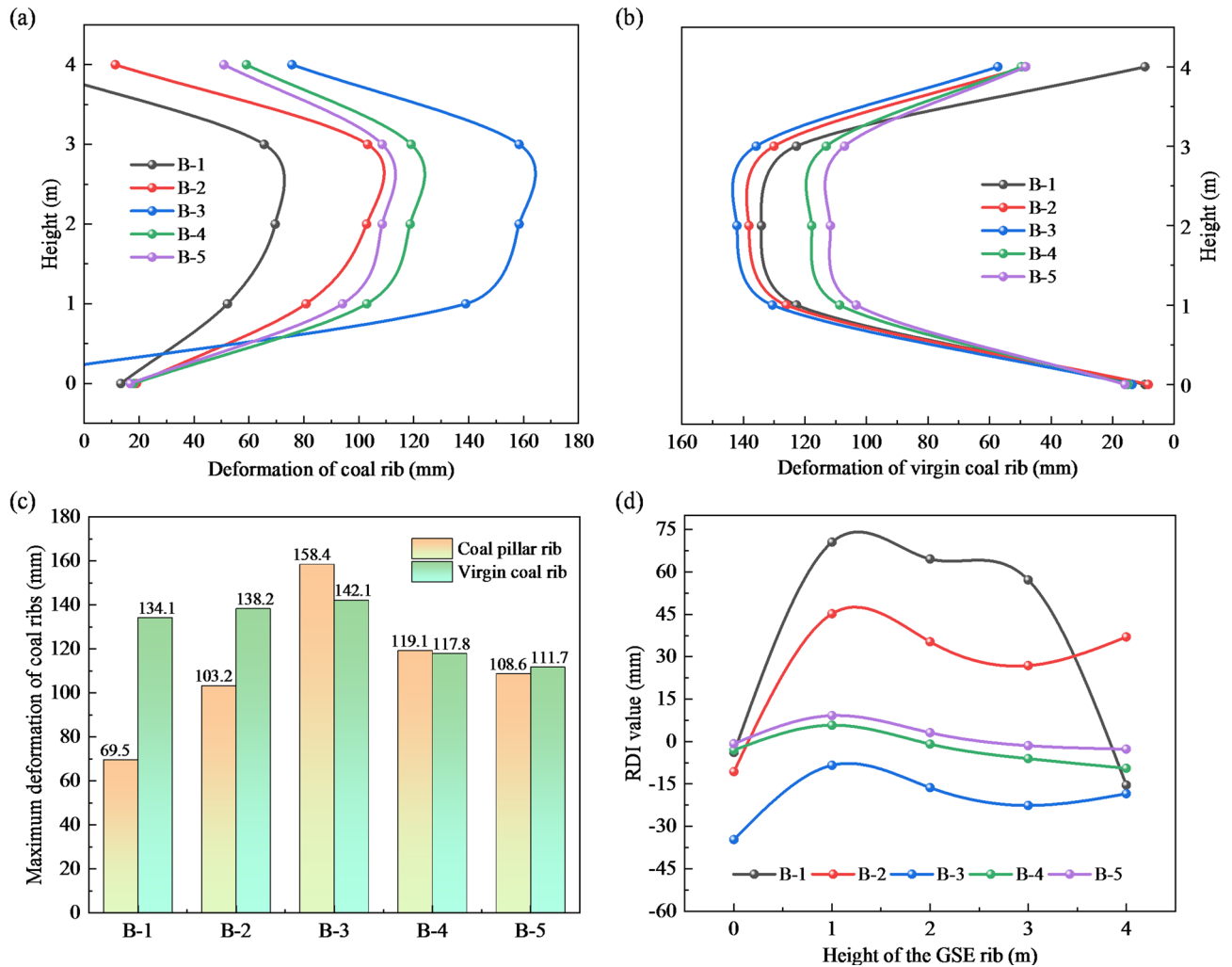


**Fig. 17.** Deformation characteristics of GSE ribs under different pillar width: (a) Deformation of the coal pillar rib; (b) Deformation of virgin coal rib; (c) Maximum value of the ribs (d) RDI value.

*Influence of excavation timing on RDI*

The GSE excavation timing refers to the lag time between the development of the GSE and the completion of mining in the upper panel. As shown by the results in Fig. 20, under the conditions of an 8 m coal pillar width and a 30 m gangue support height, when the GSE was excavated at 5e3 steps, the maximum deformations of the coal pillar rib and the virgin coal rib were 38 mm and 240 mm respectively, resulting in an RDI value of 202 mm. When the GSE excavation times were 1.5e4 steps, 2.0e4 steps, and 2.5e4 steps, the corresponding RDI values were 56 mm, 52 mm, and 50 mm, respectively. From these results, it can be inferred that the more stable the overlying rock strata are, the weaker the degree of RDI is. However, the RDI trend still exists. Even if the rock strata above the gob are completely stable, the coal ribs will still show an RDI trend when the gangue support height is great.

When the rock strata above the gob in the upper panel had not yet stabilized, they continued to subside. The cantilevered overlying strata and the coal pillar moved together towards the gob, partially offsetting the convergence of the coal pillar into the GSE. Consequently, when the GSE was excavated at 5e3 steps, the convergence of the coal pillar rib into the GSE was only 38 mm, while the deformation of the virgin coal rib reached 240 mm, resulting in a RDI of 202 mm, as shown in Fig. 21(a). In case where the overlying strata are stable, such as at 2.5e4 steps, the gob-side rib of the coal pillar is difficult to deform towards the gob and instead converges into the GSE. As a result, the RDI increment decreased to 93.3 mm, as shown in Fig. 21(b). In summary, when the supporting height of the gangue is great and the coal pillar is narrow, the GSE excavation time cannot reverse the RDI of the coal ribs, but it can affect the RDI value.

**RDI control and engineering application**

To address the RDI phenomenon caused by severe failure of coal pillars and virgin coal ribs in the GSE of Panel 8211 with an 8 m coal pillar, where the gangue support height is 30 m, four control schemes of coal ribs in GSE are proposed to resist the intense ground pressure induced by FMTCM in extra-thick coal seams. Since the

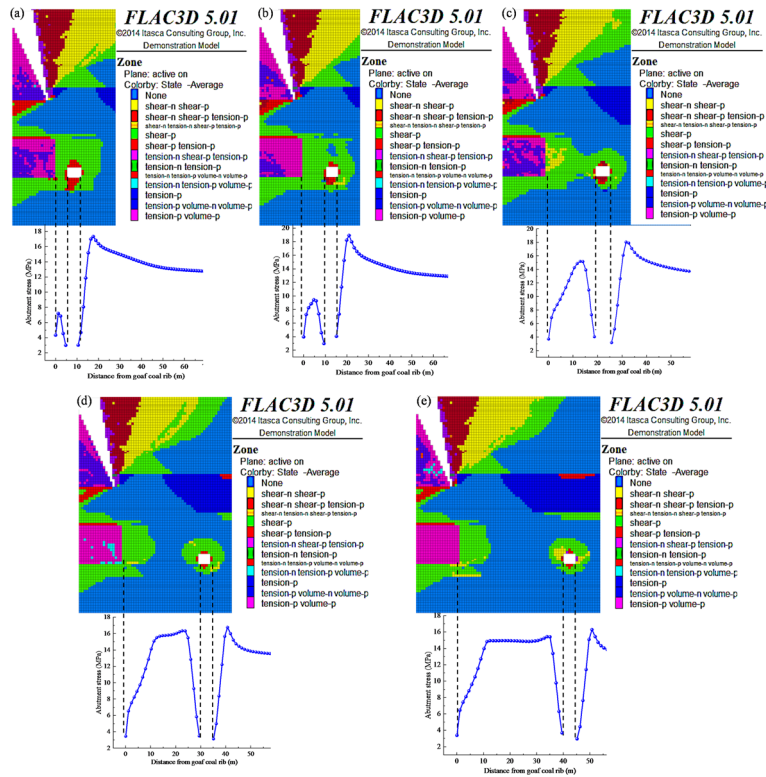


**Fig. 18.** Abutment stress of the GSE ribs with different coal pillar width at location of 450 m along GSE strike direction: (a) Group B-1; (b) Group B-2; (c) Group B-3; (d) Group B-4; (e) Group B-5.

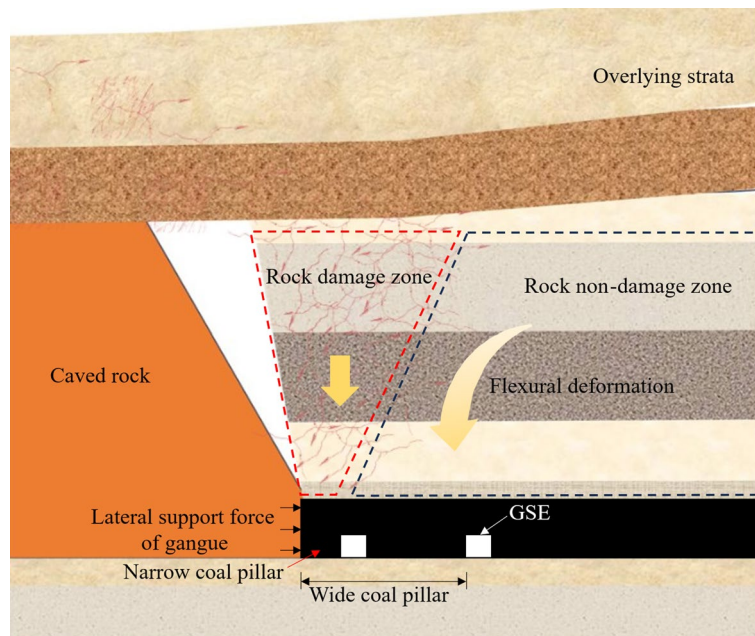


**Fig. 19.** Effect of the coal pillar width on rib deformation.

original support scheme has achieved good roof control effects, the roof in the surrounding rock control scheme still adopts the original support design, while the four rib support schemes are detailed as follows:

Scheme 1: For both the coal pillar rib and the virgin coal rib, 2000 mm bolts are adopted with identical support parameters for both ribs. The bolt spacing and row spacing are 1000 × 900 mm; the bolts adjacent to the roof and floor on the rib sides are inclined at 15° toward the roof and floor, respectively, while all other bolts are

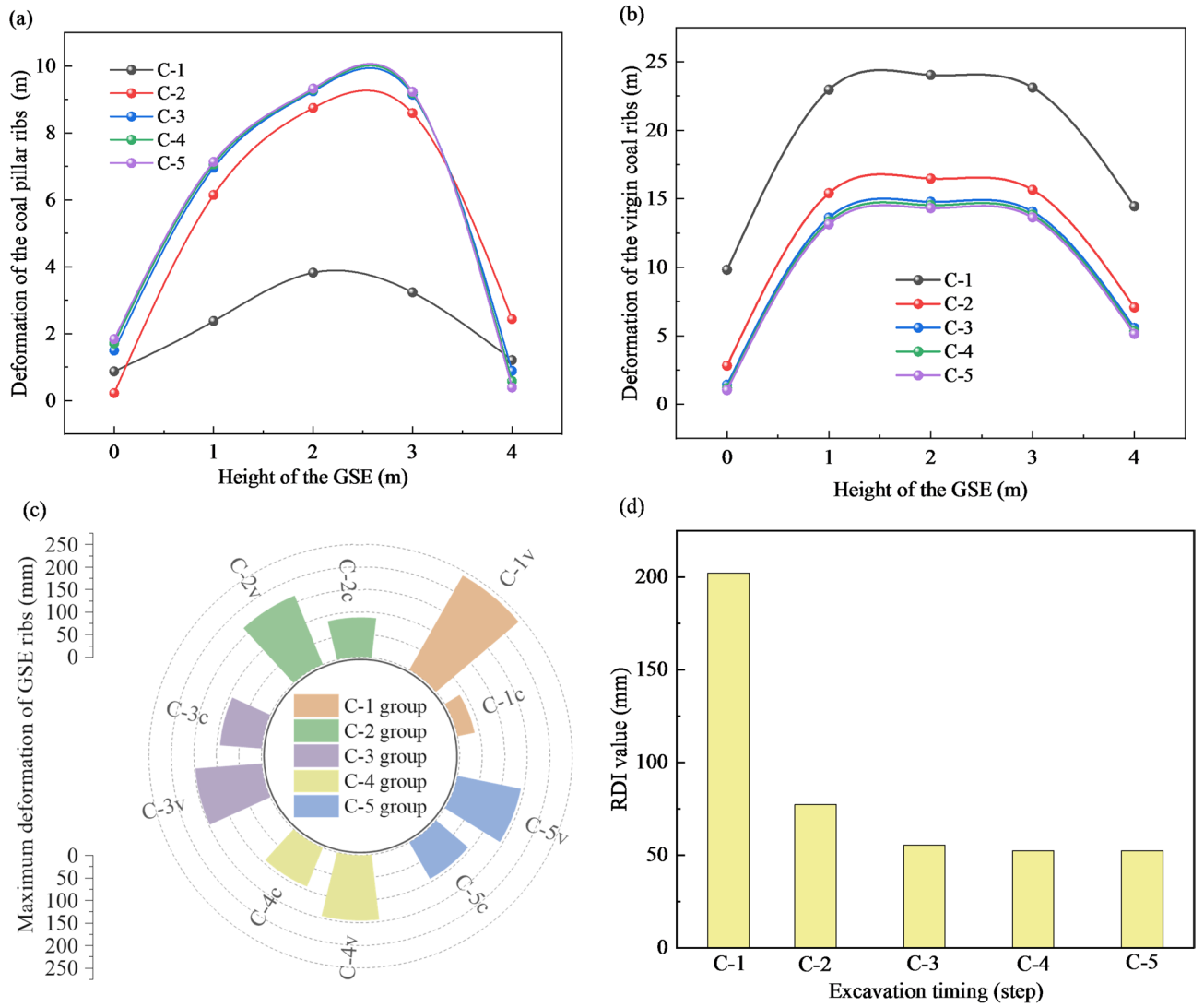


**Fig. 20.** Effect of GSE excavation timing on RDI: (a) Deformation of the coal pillar rib; (b) Deformation of the virgin coal rib; (c) Maximum deformation of GSE ribs; (d) RDI value of GSE ribs.

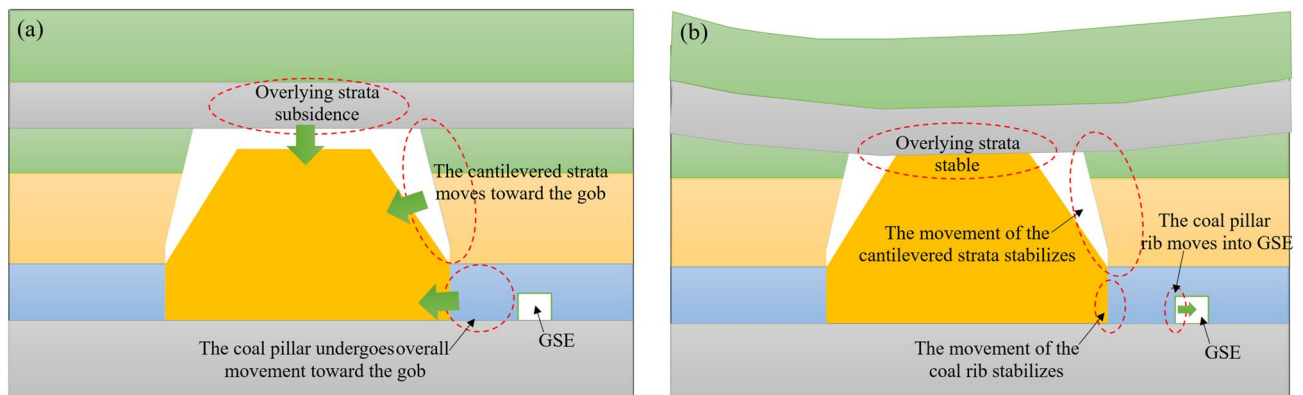


**Fig. 21.** Effect of GSE excavation timing on RDI: (a) Overlying strata unstable; (b) Overlying strata stable.

perpendicular to the coal ribs. The bolt washers have dimensions of  $120 \times 120 \times 10$  mm, and a preload of 25 kN is applied. The numerical support scheme is illustrated in Fig. 22(a).

Scheme 2: Both the coal pillar rib and the virgin coal rib are supported by 2600 mm bolts, with all other layout parameters of the bolts identical to those in Scheme 1. The numerical support scheme is illustrated in Fig. 22(b).

Scheme 3: The bolt layout is identical to that in Scheme 2. Two cables are arranged per row on the coal pillar rib: one is 1250 mm from the roof and inclined upward at  $15^\circ$ , while the other is 2300 mm from the roof and perpendicular to the coal rib. The cable length is 5250 mm, with a spacing of 1050 mm between cables and a row spacing of 900 mm. No cables are installed on the virgin coal rib. The cable washers have dimensions of  $300 \times 300 \times 16$  mm, and a prestress of 200 kN is applied. The numerical support scheme is illustrated in Fig. 22(c).

Scheme 4: Both the coal pillar rib and the virgin coal rib are supported by combined bolt and cable support. The bolt layout parameters are identical for both coal ribs: the bolt length is 3100 mm, with a spacing and row spacing of  $1000 \times 900$  mm; the bolts adjacent to the roof and floor in the ribs are inclined at  $15^\circ$  toward the roof and floor, respectively, while all other bolts are perpendicular to the coal ribs. The bolt washers have dimensions of  $130 \times 130 \times 10$  mm, and a preload of 30 kN is applied. Three cables are arranged per row on the coal pillar rib, while two cables are arranged per row on the virgin coal rib. The cable length is 5250 mm, and the diameter is 21.8 mm; the cables adjacent to the roof and floor on the coal ribs are inclined at  $15^\circ$  toward the roof and floor, respectively, and all other cables are perpendicular to the coal rib. The spacing between cables is 1050 mm with a row spacing of 900 mm in the coal pillar ribs. For the virgin coal rib, spacing between cables is 2100 mm, with a row spacing of 900 mm. The cable washers measure  $300 \times 300 \times 16$  mm, with a prestress of 200 kN applied. This numerical support scheme is illustrated in Fig. 22(d).

The numerical simulation results of the deformation of the coal pillar rib and virgin coal rib as well as the RDI under the four control schemes are illustrated in Fig. 23. During the excavation of the GSE, under Scheme 1, the deformations of the virgin coal rib and coal pillar rib are 256 mm and 196 mm, respectively, exhibiting the largest rib deformation among the four support schemes with a RDI rate of 30.6%. Compared with Scheme 1, Scheme 2 adopts longer bolts, which can reduce the rib deformation of the GSE but fails to reverse the RDI. Scheme 3 only adds cables to the coal pillar rib, achieving a reduction in the deformation of both the coal pillar rib and virgin coal rib; however, the GSE still exhibits the RDI. In contrast, under Scheme 4, where both the coal pillar rib and virgin coal rib are subjected to high-strength combined bolt and cable support, not only are the deformations of the virgin coal rib and coal pillar rib reduced to 114 mm and 149 mm, but the RDI is also successfully reversed.

During the mining of Panel 8211, the numerical results of rib deformation in the GSE under the four control schemes demonstrated the following pattern: Scheme 1 > Scheme 2 > Scheme 3 > Scheme 4. Schemes 1 to 3 all exhibited the RDI characteristic where deformation of the virgin coal rib was greater than that of the coal pillar rib, whereas under Scheme 4, RDI was not pronounced. It can thus be concluded that under Scheme 4, the deformation of the GSE is significantly reduced, and RDI is effectively controlled.

Based on the numerical simulation results, support scheme 4 was implemented in field practice to control the surrounding rock stability of the GSE, with the support parameters illustrated in Fig. 24. Under the new support scheme, the surrounding rock deformation rate of the GSE is relatively high in the early stage of excavation. The surrounding rock deformation stabilizes approximately 28 days after GSE excavation. At Monitoring Station S-1#, the stabilization deformations of the coal pillar rib and virgin coal rib are 155 mm and 140 mm, respectively (Fig. 25(a)). At Monitoring Station S-2#, the corresponding deformations are 145 mm and 135 mm respectively (Fig. 25(b)). These results indicate that the surrounding rock control technology has achieved the goal of allowing ground pressure yielding of the surrounding rock at the early stage while realizing strong control

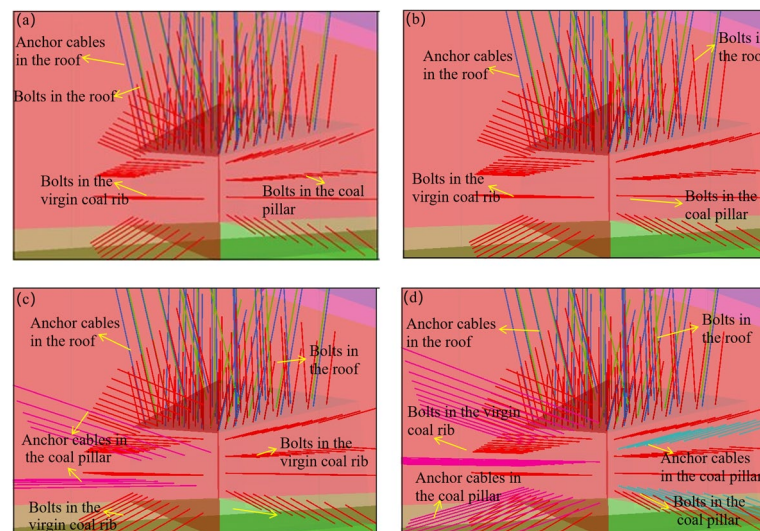


**Fig. 22.** RDI control schemes in the numerical model: (a) Scheme 1; (b) Scheme 2; (c) Scheme 3; (d) Scheme 4.

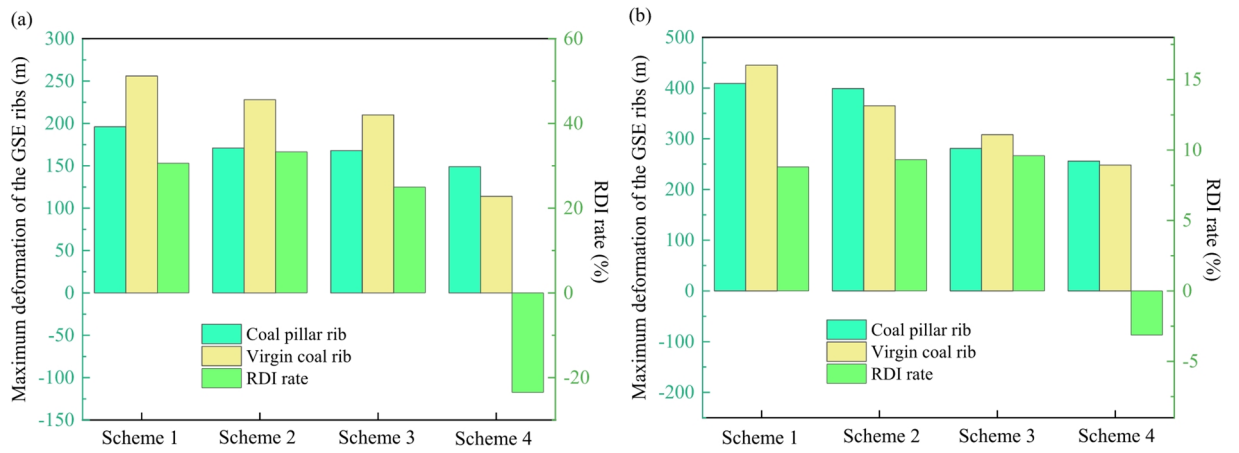


**Fig. 23.** Rib deformation and RDI rate of the GSE under different support schemes: (a) GSE excavation stage; (b) Panel 8211 mining stage.

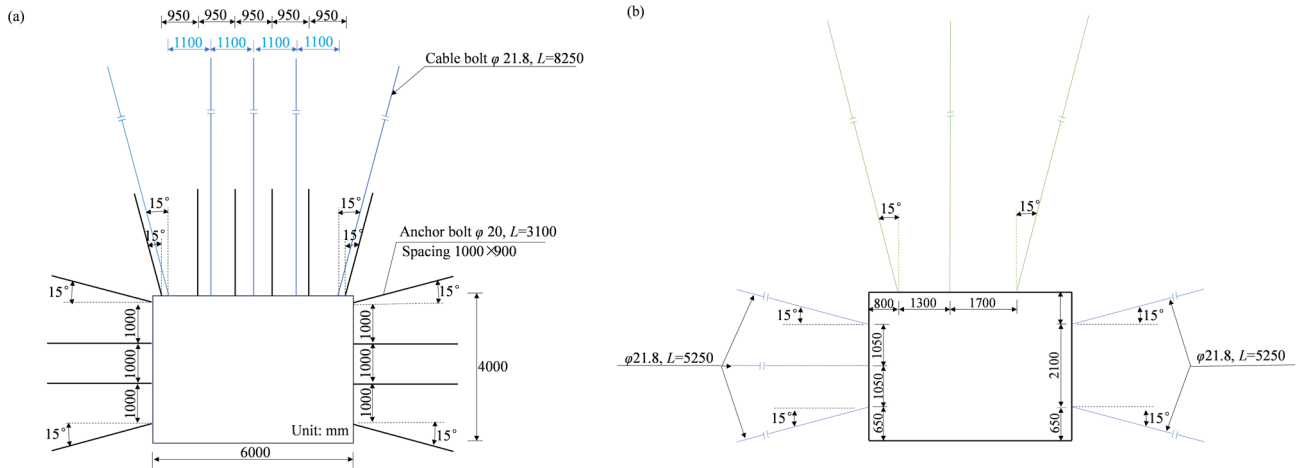


**Fig. 24.** Control Strategy for the GSE.

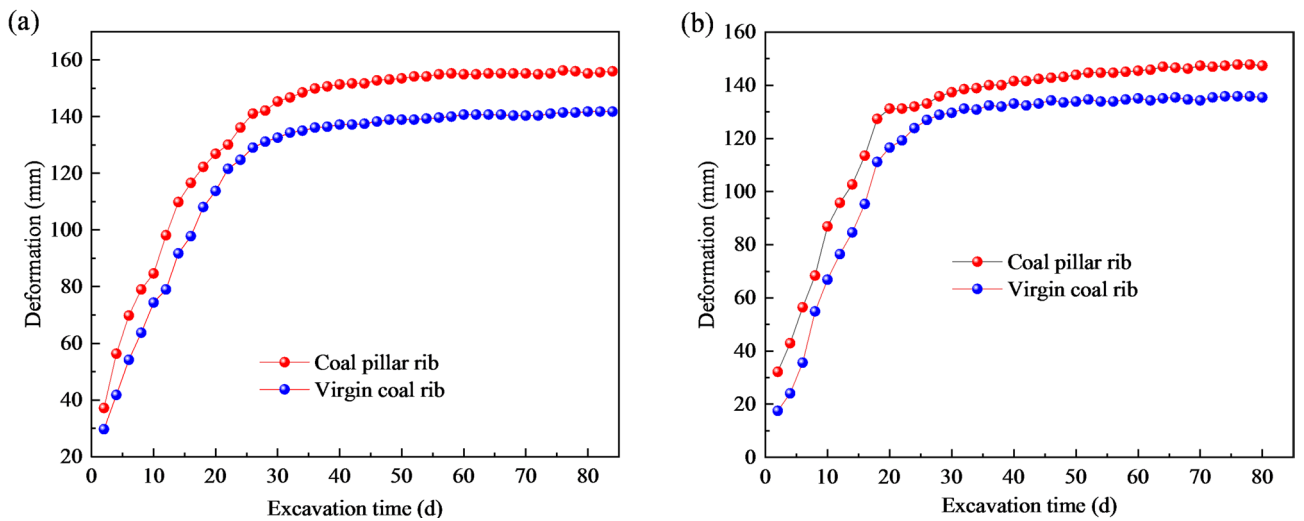


**Fig. 25.** Surrounding rock deformation under the new control scheme: (a) Station #S-1; (b) Station #S-2.



**Fig. 26.** Ground pressure control effect of the GSE.

in the later stage, and enables the overall stability of the surrounding rock to be controllable. The overall control effect is shown in Fig. 26.

### Conclusion

This study conducted investigations on a special RDI phenomenon and its mechanisms in a GSE with 8 m narrow coal pillar using FMTCM in an extra-thick coal seam of thickness 15 m and dip angle 2.5° under thick medium-coarse sandy main roof and fine sandy main floor. The research focuses on the occurrence characteristics of gangue, coal pillar width, and GSE excavation timing, while the evolution patterns of RDI under different mining-induced dynamic pressures represent an important direction for future investigation. The conclusions were drawn:

- (1) In the early stage of the excavation of the GSE with a narrow coal pillar, the traditional asymmetric deformation still occurs. Fifty days after the GSE excavation, the deformation rate of the virgin coal rib increases, and the RDI phenomenon appears.
- (2) The lateral support force of gangue to the coal pillar is the determining factor for the RDI. It leads to an increase in the horizontal and abutment stresses of the virgin coal rib. RDI occurs only when the gangue support height exceeds 20 m, and its severity plateaus above 30 m.
- (3) The coal pillar width and excavation timing of the GSE only affect the degree of RDI, rather than being the direct causes. An increase in pillar width can weaken the RDI, while the pillar width is greater than 30 m, the deformation of the coal pillar rib and the virgin coal rib is close.
- (4) A short time lag between GSE excavation and upper panel mining completion leads to instability in the overlying strata. This results in the continuous overall movement of the coal pillar toward the gob, inducing a pronounced RDI.

### Data availability

The data that support the findings of this study are available from the corresponding author upon reasonable request.

Received: 28 October 2025; Accepted: 9 January 2026

Published online: 19 January 2026

### References

1. Wu, W. D., Bai, J. B., Wang, X. Y., Yan, S. & Xu, S. X. Numerical study of failure mechanisms and control techniques for a gob-side yield pillar in the Sijiangzhuang coal mine China. *Rock Mech. Rock Eng.* **52** (4), 1231–1245. <https://doi.org/10.1007/s00603-018-1654-3> (2019).
2. Wang, J. H. et al. Key technologies and equipment for a fully mechanized top-coal caving operation with a large mining height at ultra-thick coal seams. *Int. J. Coal Sci. Technol.* **2** (2), 97–111. <https://doi.org/10.1007/s40789-015-0071-4> (2015).
3. Pan, C., Xia, B. W., Zuo, Y. J., Yu, B. & Ou, C. N. Mechanism and control technology of strong ground pressure behaviour induced by high-position hard roofs in extra-thick coal seam mining. *Int. J. Min. Sci. Technol.* **32**, 499–511. <https://doi.org/10.1016/j.ijmst.2022.01.006> (2022).
4. Peng, L. J. et al. Study on surrounding rock control technology of gob-gob roadway driven by fully mechanized caving with large mining height and small coal pillar in extra Thick coal seam. *Energy Sci. Eng.* **13**, 3422–3436. <https://doi.org/10.1002/ese3.70126> (2025).
5. Yang, H. Z., Wang, D. P., Ju, W. J., Yuan, W. M. & Su, C. Asymmetric damage mechanisms and prevention technology in large-section gob-side entry retaining. *Sustainability* **15**, 739. <https://doi.org/10.3390/su15010739> (2023).
6. Wang, B. F., Zhou, D. & Zhang, J. Research on deformation characteristics and control technology of surrounding rock for gob-side entry with small coal pillar in gently inclined coal seam. *Energy Sci. Eng.* **12**, 1759–1774. <https://doi.org/10.1002/ese3.1707> (2024).
7. Wu, H., Li, Q. F., Zhu, C. Q. & He, L. Study on the failure law of surrounding rock inclined coal seam with gob side entry. *Sci. Rep.* **13**, 973. <https://doi.org/10.1038/s41598-023-28238-3> (2023).

8. Zhu, H. Z. & Wang, H. J. Ground response of non-coal pillar mining panel. *Sustainability* **15**, 3164. <https://doi.org/10.1038/s41598-023-28238-3> (2023).
9. Zhang, L. X. et al. Evolutionary law and regulatory technology of roof migration on gob-side entry retaining. *Sci. Rep.* **14**, 5581. <https://doi.org/10.1038/s41598-023-28238-3> (2024).
10. Ma, Z. M. et al. Research on the stability mechanism of the surrounding rock of gob-side entry retaining by roof cutting in Dianping coal mine. *Minerals* **12**, 965. <https://doi.org/10.3390/min12080965> (2022).
11. Du, F. et al. Research on overburden structural characteristics and support adaptability in cooperative mining of sectional coal pillar and bottom coal seam. *Sci. Rep.* **14**, 11458. <https://doi.org/10.1038/s41598-024-62375-7> (2024).
12. Li, J., Wang, W. S., Li, B., Tan, J. H. & Peng, B. Directionality of butterfly leaves and nonuniform deformation mechanism in gob-side entry driving roadway. *J. Mech.* **37**, 291–301. <https://doi.org/10.1093/jom/ufab004> (2021).
13. Zhang, J. et al. Deformation mechanism of gob-side entry at top coal caving mining face: A numerical study. *Energy Sci. Eng.* **12**, 2456–2471. <https://doi.org/10.1002/ese3.1755> (2024).
14. Chen, D. D. et al. Application of gob-side entry driving in fully mechanized caving mining: a review of theory and technology. *Energies* **16**, 2691. <https://doi.org/10.3390/en16062691> (2023).
15. Xu, S. Q. et al. Stability mechanism and countermeasure of the solid coal rib in deep gob-side entry retaining: insights from theoretical analysis numerical simulation. *Heliyon* **10**, e24174. <https://doi.org/10.1016/j.heliyon.2024.e24174> (2024).
16. Bian, W. H., Yang, J., He, M. C., Zhu, C. & Xu, D. M. Research and application of mechanical models for the whole process of 110 mining method roof structural movement. *J. Cent. South. Univ.* **29**, 3106–3124. <https://doi.org/10.1007/s11771-022-5148-9> (2022).
17. Wang, J., Liu, P., He, M. C., Yu, G. Y. & Tian, H. Z. Floor heave mechanism for gob-side entry retaining with concrete blocks and control method: A case study. *Undergr. Space.* **15**, 244–259. <https://doi.org/10.1016/j.undsp.2023.09.002> (2024).
18. Wang, H. S. et al. Deformation mechanism and roof pre-splitting control technology of gob-side entry in Thick hard main roof full-mechanized Longwall caving panel. *J. Cent. South. Univ.* **31**, 3206–3224. <https://doi.org/10.1007/s11771-024-5719-z> (2024).
19. Zhan, X. Y. et al. Theoretical determination method and field verification of the fracture position of the main roof of the gob-side coal-rock roadway in gently inclined coal seam. *Bull. Eng. Geol. Environ.* **82**, 209. <https://doi.org/10.1007/s10064-023-03249-6> (2023).
20. Wang, M., Wang, W. Y., Xu, Y. L. & Xie, G. L. Study on the new layout pattern about the gob-side entry under dynamic pressure and its surrounding rock stability control. *Energy Sci. Eng.* **12**, 1389–1410. <https://doi.org/10.1002/ese3.1667> (2024).
21. Wang, H. S., Wang, J., Elmo, D., He, M. C. & Ma, Z. M. Ground response mechanism of entries and control methods induced by hard roof in Longwall top coal caving panel. *Eng. Fail. Anal.* **144**, 106940. <https://doi.org/10.1016/j.engfailanal.2022.106940> (2023).
22. Wang, W., Wu, Y. H., Lu, X. W. & Zhang, G. J. Study on small coal pillar in gob-side entry driving and control technology of the surrounding rock in a high-stress roadway. *Front. Earth Sci.* **10**, 1020866. <https://doi.org/10.3389/feart.2022.1020866> (2023).
23. Li, G. Y., Gao, L. S., Ma, Q. & Liu, H. R. Research on the optimization and application of coal pillar width in gob-side entry driving under hard roof condition. *Front. Earth Sci.* **13**, 1603252. <https://doi.org/10.3389/feart.2025.1603252> (2025).
24. Wang, D. Q. et al. Study on surrounding rock failure mechanism and rational coal pillar width of the gob-side coal roadway under influence of intense dynamic pressure. *Energy Sci. Eng.* **11**, 1716–1733. <https://doi.org/10.1002/ese3.1416> (2023).
25. Li, G. J., Wang, X. Y., Bai, J. B., Wu, B. W. & Wu, W. D. Research on the failure mechanism and control technology of surrounding rock in gob-side entry driving under unstable overlying strata. *Eng. Fail. Anal.* **138**, 106361 (2022).
26. Xu, X. H., He, F. L., Li, X. B. & He, W. R. Research on mechanism and control of asymmetric deformation of gob side coal roadway with fully mechanized caving mining. *Eng. Fail. Anal.* **120**, 105097. <https://doi.org/10.1016/j.engfailanal.2020.105097> (2021).
27. Xu, J. H. et al. Overlying main roof breaking characteristic and its effect on the stability of gob-side entry. *Geomech. Geophys. Geo-energy* **9**, 26. <https://doi.org/10.1007/s40948-023-00566-8> (2023).
28. Cao, Z. Z. et al. Disaster-Causing mechanism of spalling rock burst based on folding catastrophe model in coal mine. *Rock Mech. Rock Eng.* **58**, 7591–7604. <https://doi.org/10.1007/s00603-025-04497-6> (2025).
29. Han, Z. P. et al. Mechanism of rock burst in deep gob-side entry based on dynamic and static stress: A case study. *Geomatics Nat. Hazards Risk.* **14** (1), 2271636. <https://doi.org/10.1080/19475705.2023.2271636> (2023).
30. Liu, H. D., Liu, C. Y. & Dong, Y. N. Theoretical study on the mechanism of asymmetrical large deformation of heading roadway facing mining. *Sustainability* **14**, 15065. <https://doi.org/10.3390/su142215065> (2022).
31. Wang, Q. et al. Comparative study of model tests on automatically formed roadway and gob-side entry driving in deep coal mines. *Int. J. Min. Sci. Technol.* **31** (4), 591–601. <https://doi.org/10.1016/j.ijmst.2021.04.004> (2021).
32. Zhao, Y. X., Zhou, J. L., Zhang, C. & Liu, B. Failure mechanism of gob-side roadway in deep coal mining in the Xinjie mining area: theoretical analysis and numerical simulation. *J. Cent. South. Univ.* **30**, 1631–1648. <https://doi.org/10.1007/s11771-023-5315-7> (2023).
33. Wu, W. D. et al. Failure characteristics and cooperative control strategies for gob-side entry driving near an advancing working face: a case study. *Processes* **12**, 1398. <https://doi.org/10.3390/pr12071398> (2024).
34. Xie, S. R. et al. Research on the control technology and key parameters of external anchor-internal unloading of surrounding rock during gob-side entry driving under severe mining of 1000-m-deep mine. *Rock. Mech. Eng.* **57**, 2913–2932. <https://doi.org/10.1007/s00603-023-03722-4> (2024).
35. Chong, J. et al. Mining pressure distribution law and disaster prevention of isolated Island working face under the condition of hard umbrella arch. *Rock Mech. Rock Eng.* **57**, 8323–8341. <https://doi.org/10.1007/s00603-024-03961-z> (2024).
36. Lv, J. K. et al. Effect of multi-factor dynamic loading on gob-side entry driving during Longwall face extraction: A case study. *Bull. Eng. Geol. Environ.* **81**, 409. <https://doi.org/10.1007/s10064-022-02880-z> (2022).
37. Mu, Z. L. et al. The role of mining-induced seismicity amplitude and frequency in gob-side roadway rib spalling. *Energy Explor. Exploit.* **43** (1), 79–104. <https://doi.org/10.1177/01445987241266890> (2025).
38. Li, H. et al. Study on the stability of coal pillars in a gob-side two-entry arrangement of different layers in fully mechanized caving and the zonal linkage control of heteromorphic surrounding rock. *Processes* **11**, 1806. <https://doi.org/10.3390/pr11061806> (2023).
39. Jiang, Z. S., Guo, W. K. & Xie, S. R. Coal pillar size determination and surrounding rock control for gob-side entry driving in deep soft coal seams. *Processes* **11**, 2331. <https://doi.org/10.3390/pr11082331> (2023).
40. Wang, J. Y. et al. Stress and deformation evolution characteristics of gob-side entry retained by roof cutting and pressure relief. *Tunn. Undergr. Space Technol. Incorporating Trenchless Technol. Res.* **123**, 104419. <https://doi.org/10.1016/j.tust.2022.104419> (2022).
41. Hoek, E. & Brown, E. T. Practical estimates of rock mass strength. *Int. J. Rock Mech. Min. Sci.* **34**, 1165–1186. [https://doi.org/10.1016/s1365-1609\(97\)80069-x](https://doi.org/10.1016/s1365-1609(97)80069-x) (1997).
42. Hoek, E. & Brown, E. T. *Underground Excavation in Rock* (The Institute of Mining and Metallurgy, 1980).
43. Ma, X. et al. Failure mechanism of severe deformation in gob-side entry rib and unloading-supporting coupling control technology. *Eng. Fail. Anal.* **167**, 108973. <https://doi.org/10.1016/j.engfailanal.2024.108973> (2024).
44. Zhang, H. W. et al. Stability control of narrow coal pillars in the fully-mechanized gob-side entry during sequenced top coal caving mining. *J. China Coal Soc.* **46** (4), 1211–1219. <https://doi.org/10.13225/j.cnki.jccs.2020.0028> (2021).

## Acknowledgements

The authors are thankful to the financial support from Zhejiang Provincial Natural Science Foundation (Grant No. LQN26E040007), China Postdoctoral Science Foundation (Grant No. 2024M763553), Scientific Research

Fund of Zhejiang Provincial Education Department (Grant No. Y202352229), Housing and Urban-Rural Development Department of Zhejiang (Grant No. 2024AY40014), and Youth Project of Jiaxing Science and Technology Program (Grant No. 2024AY40014).

### Author contributions

Wenrui He contributed to data curation, funding acquisition, investigation, methodology development, software implementation, and writing both the original draft and the review & editing of the manuscript. Dongdong Chen was involved in conceptualization, resource provision, and validation. Hengzhong Zhu contributed to investigation, supervision, and validation.

### Funding

Zhejiang Provincial Natural Science Foundation (Grant No. LQN26E040007), China Postdoctoral Science Foundation (Grant No. 2024M763553), Scientific Research Fund of Zhejiang Provincial Education Department (Grant No. Y202352229), Housing and Urban-Rural Development Department of Zhejiang (Grant No. 2024AY40014), and Youth Project of Jiaxing Science and Technology Program (Grant No. 2024AY40014).

### Competing interests

The authors declare no competing interests.

### Additional information

**Correspondence** and requests for materials should be addressed to W.H. or H.Z.

**Reprints and permissions information** is available at [www.nature.com/reprints](http://www.nature.com/reprints).

**Publisher's note** Springer Nature remains neutral with regard to jurisdictional claims in published maps and institutional affiliations.

**Open Access** This article is licensed under a Creative Commons Attribution-NonCommercial-NoDerivatives 4.0 International License, which permits any non-commercial use, sharing, distribution and reproduction in any medium or format, as long as you give appropriate credit to the original author(s) and the source, provide a link to the Creative Commons licence, and indicate if you modified the licensed material. You do not have permission under this licence to share adapted material derived from this article or parts of it. The images or other third party material in this article are included in the article's Creative Commons licence, unless indicated otherwise in a credit line to the material. If material is not included in the article's Creative Commons licence and your intended use is not permitted by statutory regulation or exceeds the permitted use, you will need to obtain permission directly from the copyright holder. To view a copy of this licence, visit <http://creativecommons.org/licenses/by-nc-nd/4.0/>.

© The Author(s) 2026